Acta Geologica Sinica (English Edition), 2019, 93(6): 1947–1966

REVIEWS

Advances in Research of Mineral Chemistry of Magmatic and Hydrothermal Biotites

TANG Pan[1], CHEN Yuchuan[2], TANG Juxing[2, *], WANG Ying[1], ZHENG Wenbao[2, 3], LENG Qiufeng[4], LIN Bin[2] and WU Chunneng[5]

[1] *Faculty of Geosciences and Environmental Engineering, Southwest Jiaotong University, Chengdu 611756, China*
[2] *Institute of Mineral Resources, Chinese Academy of Geological Sciences (CAGS), Beijing 100037, China*
[3] *China University of Geosciences, Beijing 100083, China*
[4] *Guangxi Nonferrous Metal Group Resource Exploration Co., Ltd., Nanning 530023, China*
[5] *College of Earth Sciences, Chengdu University of Technology, Chengdu 610059, China*

Abstract: Biotite is an important hydrated ferromagnesian silicate mineral in igneous rocks and porphyry deposits. The determination of chemical compositions of biotite plays an important role in both igneous petrology and ore forming processes. This paper summarizes research results of magmatic and hydrothermal biotites exemplified by the Lakange porphyry Cu–Mo deposit and the Qulong porphyry Cu deposit in the Gangdese porphyry–skarn metallogenic belt, Tibet. Biotite mineral chemistry can provide critical insights into classification, geothermometer, geothermobarometry, oxygen fugacity, petrogenesis and tectonic setting, evaluating magmatic-hydrothermal process by halogen and halogen fugacity ratios, and distinguishing between barren and mineralized rocks. Biotite provides the latest mineralogical evidence on metallogenic prognosis and prospecting evaluation for porphyry Cu polymetallic deposits or magmatic hydrothermal deposits.

Key words: magmatic biotites, hydrothermal biotites, mineral chemistry, porphyry deposit, Lakange, Qulong, Gangdese

Citation: Tang et al., 2019. Advances in Research of Mineral Chemistry of Magmatic and Hydrothermal Biotites. Acta Geologica Sinica (English Edition), 93(6): 1947–1966. DOI: 10.1111/1755-6724.14395

1 Introduction

Since the quantitative chemical analysis was introduced in mineral chemistry in late 1950s, mineralogy has gradually perfected in the analysis test and microscopic observation means. Compared with the mineral separation analysis, the mineral in situ microanalysis, such as electron microprobe (EMPA), ion microprobe (IMA) and laser plasma mass spectrometry (LA-ICP-MS), can effectively avoid the influence of mineral part alteration, impurities and inclusions.

Biotite, a trioctahedral mica with generalized formula (K, Na, Ca, Ba)(Fe^{2+}, Fe^{3+}, Mg, Ti^{4+}, Mn, Al)$_3$(Al, Si)$_4O_{10}$ (OH, F, Cl)$_2$, is an important hydrated ferromagnesian silicate in igneous rocks and porphyry deposits (Jacobs et al., 1976, 1979). In such environments, most biotite has formed during the crystallization of igneous rocks or during hydrothermal alteration (Jacobs et al., 1976, 1979). The chemical composition of biotite is sensitive to chemical and physical factors associated with early magmatic to subsequent hydrothermal activity, including the concentration of water, halogens, ore metals, oxidation states and sulfidation equilibria, volatile phase exsolution melt-fluid-vapor elemental partitioning relations and complexing at the range of temperatures and pressures of ore formation (Wones et al., 1965; Czamanske et al., 1973; Speer, 1987). Chemical variation of biotite from magmatic and associated hydrothermal alteration has been subjected to numerous studies (Beane, 1974; Jacobs et al., 1976, 1979; Hendry et al., 1981, 1985; Chivas, 1981; Selby et al., 2000; Ayati et al., 2008; Boomeri et al., 2009, 2010; Afshooni et al., 2013; Parsapoor et al., 2015; Tang et al., 2019).

In the Chinese literature, there are many studies on magmatic biotites (Hong et al., 1982; Zhou et al., 1986; Zhang et al., 1991; Wang et al., 1998; Xiong et al., 2001; Hu et al., 2006; Lou et al., 2006; Li et al., 2007a, 2007b; Qin et al., 2009; Liu et al., 2010; Zhang et al., 2011; Mi et al., 2014; Guo et al., 2015; Tao et al., 2015; Niu et al., 2015; Wu et al., 2015; Chen et al., 2015), but less on hydrothermal biotites associated with hydrothermal alteration (Yang, 1964; Fu, 1981; Liu et al., 1984; Wang et al., 2012; Tang et al., 2016). Based on the research of predecessors and author, using the large Lakange porphyry Cu–Mo deposit and the Qulong porphyry Cu deposit in the Gangdese porphyry–skarn metallogenic belt, Tibet, as examples, this article systematically summarizes advances in research of biotite mineral chemistry in order to further promote the in-depth study of biotite minerals chemistry, and provide the basic data of prospecting mineralogy and genetic mineralogy research for porphyry Cu polymetallic deposits.

* Corresponding author. E-mail: tangjuxing@126.com

© 2019 Geological Society of China

2 Biotite Classification

2.1 Genetic classification

Biotite is divided into magmatic and hydrothermal biotite (Jacobs et al., 1976, 1979; Fu, 1981). The term "magmatic" refers to biotites crystallized directly from a silicate melt, whereas hydrothermal biotite forms during hydrothermal alteration. Magmatic biotite occurs as euhedral to subhedral phenocrysts and microphenocrysts, and subhedral to anhedral flakes. Some magmatic biotites are ragged, splintery, or frayed. Magmatic biotite phenocrysts parcel magnetite, apatite, sphene, zircon and other accessory mineral in early crystallization. Magmatic biotite phenocrysts frequently are partially altered to hydrothermal chlorite or fine-grained hydrothermal biotite along their edges and cracks (Figs. 1a–c, Figs. 2a–b).

Hydrothermal biotite is further subdivided into replacement biotite, i.e., replacement of amphiboles and magmatic biotiteand less of plagioclase, and neoformed biotite, i.e., other hydrothermal biotite outside replacement biotite (Jacobs et al., 1976, 1979; Fu, 1981). Replacement biotite, anhedraal-subhedral crystal, forms by the partial or complete replacement of amphiboles and magmatic biotite, as recrystallized to fine-grained flakes in an aggregate along their edges and cracks (Figs. 1c–e, Fig. 2a).

Neoformed biotite is divided into veinlet and disseminated secondary biotites (Jacobs et al., 1976, 1979). Disseminated secondary biotite occurs as very fine to fine-grained flakes or aggregates of a few such flakes disseminated throughout the rock (Figs. 1f–h, Figs. 2c–d). In most occurrences this type of biotite is clearly associated with hydrothermal alteration. However, in rocks having little or no visible evidence of hydrothermal alteration, the grains of biotite that match closely the texture of disseminated secondary biotite can be either magmatic or hydrothermal, or a mixture of the two. Veinlet biotite, anhedraal-subhedral-euhedral crystal, most commonly occurs as very coarse to medium-grained flakes, and frequently symbiosis with quartz and sulfides (Fig. 1j, Figs. 2e–f).

Petrographic criteria and chemical compositions can distinguish magmatic and hydrothermal biotites. Beane (1974) studied biotites from North American porphyry copper deposits and concluded that magmatic biotites generally have molecular ratios of Mg/Fe <1.0, whereas hydrothermal biotites appear to be characterized by Mg/Fe >1.5 and Fe^{+3}/Fe^{+2} <0.3, and then used the Fe^{+3}–Fe^{+2}–Mg^{+2} ternary to distinguish between magmatic and hydrothermal biotites. Nachit et al. (2005) used the TiO_2–FeO^*–MgO

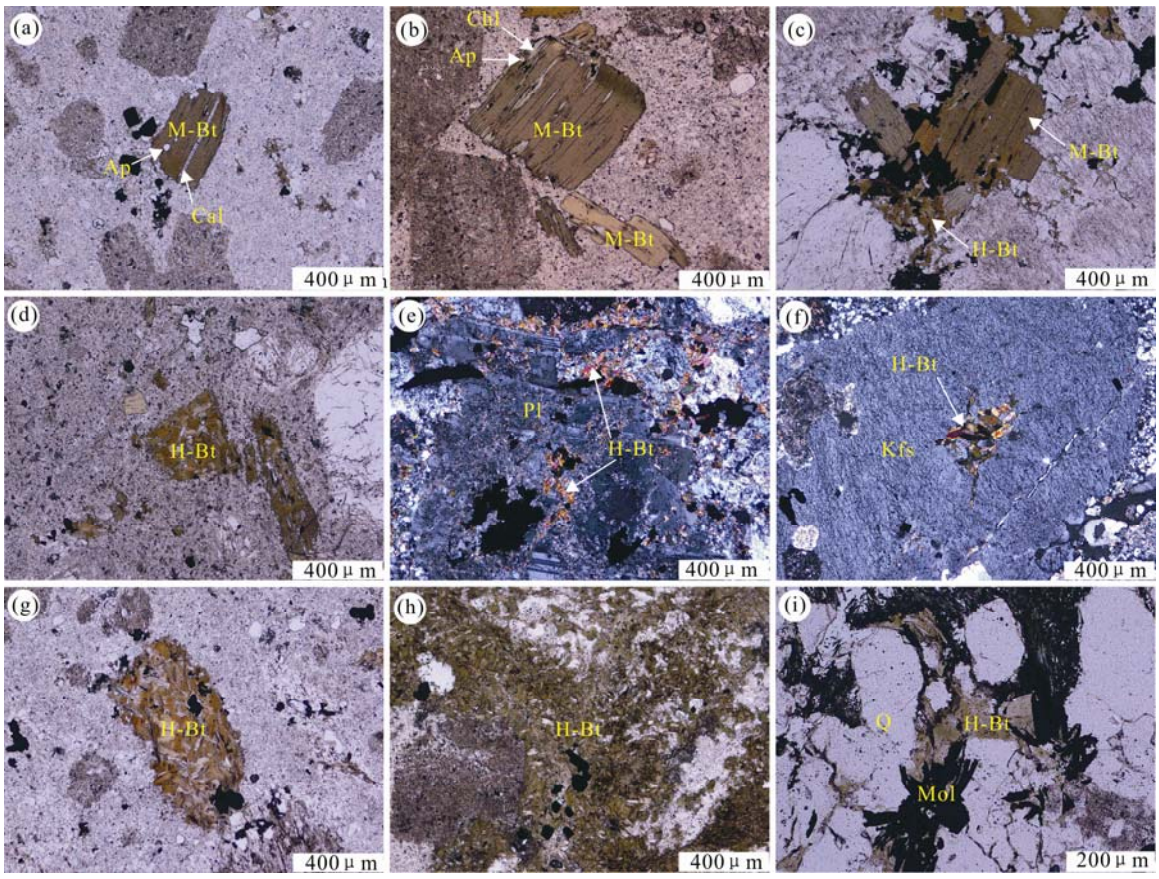


Fig. 1. Photomicrographs of biotites in the Lakange porphyry Cu–Mo deposit.

(a) ZK101-26.7 granodiorite-porphyry: magmatic biotite (M-Bt), parceling early crystallized apatite (Ap), altered to calcite (Cal); (b) ZK001-378 granodiorite-porphyry: magmatic biotite altered to chlorite (Chl); (c) ZK101-435.7 granodiorite-porphyry: magmatic biotite altered to hydrothermal biotite (H-Bt); (d) ZK201-321 granodiorite-porphyry: fine-grained biotite, and the pseudomorphs of amphibole phenocryst; (e) ZK101-435 granodiorite-porphyry: plagioclase (Pl) altered to hydrothermal biotite; (f) ZK001-275 granodiorite-porphyry: k-feldspar (Kfs) altered to hydrothermal biotite; (g) ZK201-399 granodiorite-porphyry: hydrothermal biotite in aggregates; (h) ZK 001-63.4 granodiorite-porphyry: disseminated hydrothermal biotite; (i) ZK101-439 granodiorite-porphyry: hydrothermal biotite in quartz (Q) + molybdenite (Mol) vein.

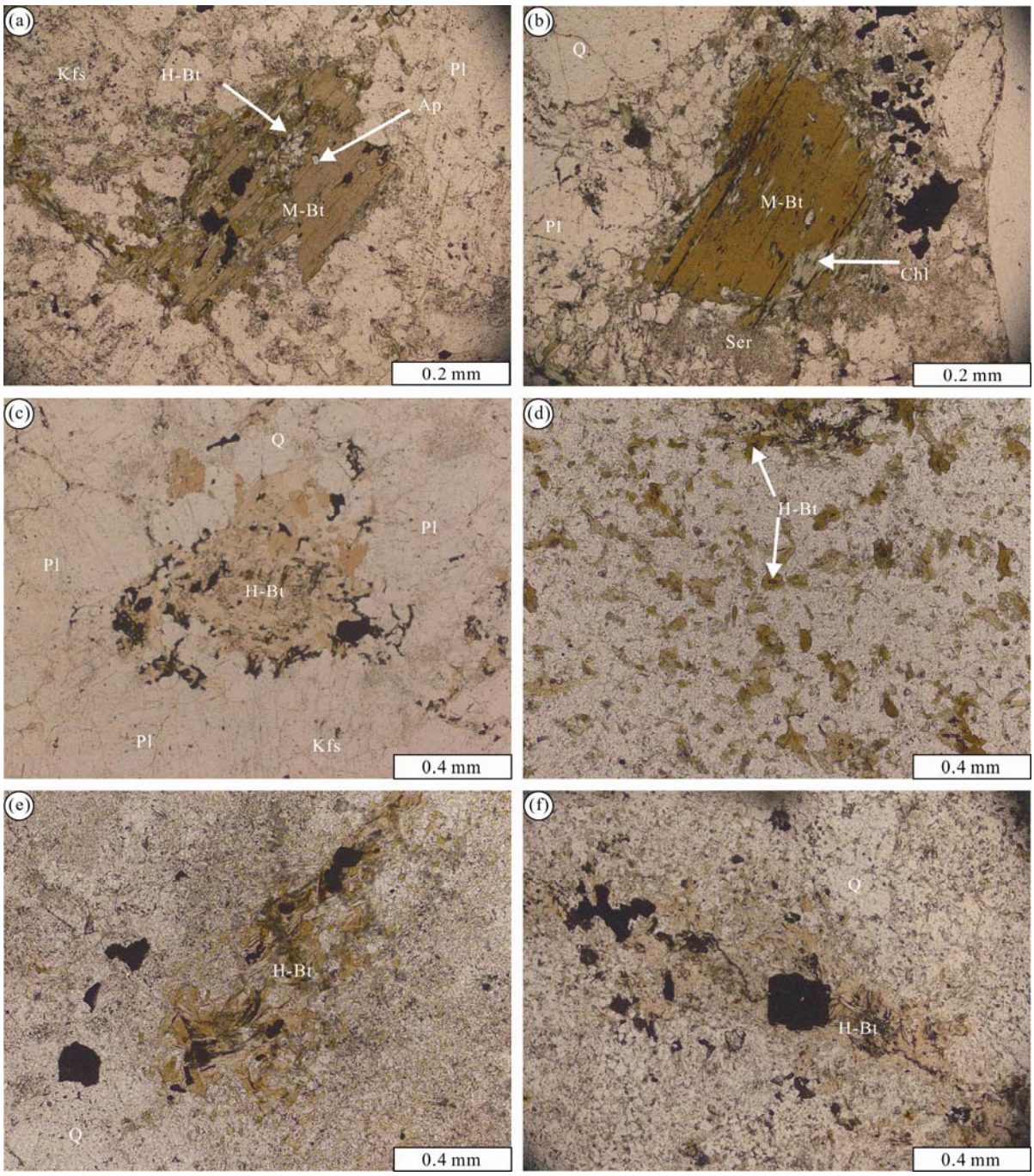


Fig. 2. Photomicrographs of biotites in the Qulong porphyry Cu–Mo deposit.
(a) ZK012-118 monzonitic granite: magmatic biotite (M-Bt), parceling early crystallizaed apatite (Ap), partially replaced by hydrothermal biotite (H-Bt); (b) ZK001-281.8 monzonitic granite porphyry: magmatic biotite altered to chlorite (Chl), plagioclase (Pl) replaced by sericite (Ser); (c) ZK015-498.8 monzonitic granite: hydrothermal biotite in aggregates; (d) ZK015-280.8 monzonitic granite: disseminated hydrothermal biotite; (e) ZK009-282 monzonitic granite porphyry: hydrothermal biotite in vein; (f) ZK005-254 monzonitic granite porphyry: hydrothermal biotite in vein; Kfs- K-feldspar; Q- Quartz.

ternary (FeO^*=FeO+MnO) to distinguish between primary magmatic, reequilibrated and neoformed biotites. FeO^*, MgO and TiO_2 were selected for the following reasons. 1) The two end-members of biotites are phlogopite (Mg) and annite (the Fe^{2+} equivalent). 2) $X_{FeO*}=FeO^*/(FeO^*+MgO)$ of biotites depends on that of the host rock; it increases from $X_{FeO*}\approx0$ in basic rocks to $X_{FeO*}\approx1$ in felsic ones (Abrecht et al., 1988). 3) The Ti content of biotites is thermo-dependent (Robert, 1976), and varies with the X_{FeO*} of the host-rock (Abrecht et al., 1988). 4) The alteration of biotites, already visible by optical microscopic methods (discolouring, pleochroism decrease, etc.) is frequently associated with a neocrystallization of Fe–Ti oxides (rutile, anatase and ilmenite).

Fu (1981), based on biotite data from several Chinese porphyry copper deposits, concluded that magmatic biotites have high titanium content (TiO_2 >3%) and low aluminum content (Al_2O_3 <15%), whereas neoformed

biotites have low titanium content (TiO_2 <3% and mostly <2%) and high aluminum content (Al_2O_3 >15%). The titanium and aluminum contents of replacement biotite are between the former two. It indicates that elements are hereditability in the process of replacement. Magmatic biotites have higher Ti content than hydrothermal biotites mainly because the concentration of Ti in biotites is very sensitive to temperature (Robert, 1976).

Jacobs and Parry (1976, 1979) studied the Santa Rita, Bingham and Ely porphyry deposits and concluded that magmatic biotite is distinguished from hydrothermal biotite by its higher Ba content; furthermore, hydrothermal biotite is Mg-rich and F-rich, and Ti-poor. Bea et al. (1994) showed that Ba in granitic magma is hosted in biotite and potassium feldspar in the form of isomorphism, and Ba substitutes for K or Ca in biotite early and in K-feldspar late in the magma evolution. In the process of magmatic hydrothermal evolution, therefore, the Ba content in biotite is less and less. Therefore, the Ba content in magmatic biotite is higher than that of hydrothermal biotite.

There are magmatic and hydrothermal biotite in the Lakange porphyry Cu–Mo deposit and the Qulong porphyry Cu deposit (Figs. 1 and 2). The elemental analyses of biotites from the Lakange porphyry Cu–Mo deposit and the Qulong porphyry Cu deposit were obtained from doubly polished thin sections using a EPMA-1600 electron microprobe made by Shimadzu at the Tianjin Center, China Geological Survey. The analyses were conducted using a 15 kV accelerating voltage, 20 nA beam current and 10 μm beam diameter. The biotite formulas were calculated on the basis of 22 oxygen atoms, and the Fe^{3+} and Fe^{2+} were estimated by the method proposed by Lin et al. (1994). The analyses of biotites from the two deposits are shown in Table 1 and Table 2.

In the Lakange deposit, hydrothermal biotites from the potassic zone have high Si content (5.84–6.16, mean=6.02), whereas magmatic biotites and hydrothermal biotites from the phyllic zone have low Si content, i.e., 5.63–5.99, mean=5.78 and 5.52–6.02, mean=5.80, respectively. Magmatic biotites have high Ti content (0.34 –0.41, mean=0.38), whereas hydrothermal biotites from the potassic and the phyllic zone have low Ti content, i.e., 0.18–0.31, mean=0.24 and 0.19–0.33, mean=0.27, respectively. Hydrothermal biotites from the potassic zone have high Mg content (3.87–4.29, mean=4.02), whereas magmatic biotites and hydrothermal biotites from the phyllic zone have low Mg content, i.e., 3.13–3.49, mean=3.28 and 2.96–3.93, mean=3.42, respectively. Hydrothermal biotites from the potassic zone have low Fe content (0.99–1.52, mean=1.28), whereas magmatic biotites and hydrothermal biotites from the phyllic zone have high Fe content, i.e., 1.70–2.18, mean=1.99 and 1.34 –2.18, mean=1.78, respectively. The TiO_2 and BaO contents of magmatic biotites from the Lakange porphyry Cu–Mo deposit are 2.98%–3.52% (mean=3.27%) and 0.09%–0.63% (mean=0.28%) respectively, whereas in hydrothermal biotites, the TiO_2 and BaO contents are 1.57%–2.74% (mean=2.23%) and 0%–0.11% (mean= 0.04%) respectively.

In the Qulong deposit, magmatic biotites have high Ti content (0.30–0.99, mean=0.42), whereas hydrothermal biotites from the potassic and phyllic zones have low Ti content, i.e., 0.17–0.33, mean=0.25 and 0.18–0.29, mean=0.22, respectively. Hydrothermal biotites from the potassic zone have high Mg content (3.71–4.53, mean=4.06), whereas magmatic biotites and hydrothermal biotites from the phyllic zone have low Mg content, i.e., 3.07–4.18, mean=3.70 and 3.21–3.78, mean=3.47, respectively. Hydrothermal biotites from the potassic zone have low Fe content (0.64–1.44, mean=1.06), whereas magmatic biotites and hydrothermal biotites from the phyllic zone have high Fe content, i.e., 0.91–2.18, mean=1.36 and 1.08–2.09, mean=1.61, respectively. The TiO_2 and BaO contents of magmatic biotites in the Qulong porphyry Cu deposit are 2.68%–9.24% (mean=3.74%) and 0.22%–0.66% (mean= 0.49%) respectively, whereas in hydrothermal biotites, the TiO_2 and BaO contents are 1.54%–2.98% (mean=2.15%) and 0%–0.13% (mean= 0.04%), respectively.

Magmatic biotites have higher Ti and Ba contents than hydrothermal biotites in the Lakange deposit and the Qulong deposit. Magmatic biotites are also Ti-rich in the Darreh-Zar porphyry Cu deposit and Jiama porphyry Cu polymetallic deposit (Parsapoor et al., 2015; Tang et al, 2016), and Ba-rich in the Santa Rita, Bingham, Ely, and Darreh-Zar porphyry deposits (Jacobs et al., 1976, 1979; Parsapoor et al., 2015). Therefore, the Ba and Ti contents in biotite can be used to distinguish magmatic and hydrothermal biotites.

2.2 Composition classification

According to the International Mineralogical Association (IMA) classification scheme, biotite is divided into four end members: annite [$KFe^{2+}{}_3AlSi_3O_{10}(OH)_2$], phlogopite [$KMg_3AlSi_3O_{10}(OH)_2$], siderophyllite [$KFe^{2+}{}_2AlAlSi_2O_{10}(OH)_2$] and eastonite [$KMg_2AlAlSi_2O_{10}(OH)_2$] (Rieder et al., 1998). There are five biotite classification diagrams, including Mg–(Al^{VI}+Fe^{3+}+Ti)–(Fe^{2+}+Mn) diagram (Foster, 1960), (Mg–Li)–(Fe^{tot}+Mg+Ti –Al^{VI}) diagram (Tischendorf et al., 1997), ΣAl(apfu)–Fe/(Fe+Mg) diagram (Rieder et al., 1998), Fe/(Fe+Mg)–Al^{VI}diagram (Deer et al., 1992) and Si–Mg/(Mg+Fe^{2+}+Fe^{3+}+Mn) diagram (Kanisawa, 1983). The first two are the most.

According to the nomenclature of Foster (1960) and Tischendorf et al. (1997), biotites from the phyllic zone and magmatic biotites in the Lakange porphyry Cu–Mo deposit plot in the Mg-biotite field of the Mg–(Al^{VI}+Fe^{3+}+Ti)–(Fe^{2+}+Mn) and (Mg–Li)–(Fe^{tot}+Mn+Ti–Al^{VI}) diagrams, whereas biotites from the potassic zone plot in the Mg-biotite and phlogopite fields (Fig. 3a–b). Biotites from the phyllic zone and magmatic biotites in the Qulong porphyry Cu deposit plot in the Mg-biotite and phlogopite fields of Mg–(Al^{VI}+Fe^{3+}+Ti)–(Fe^{2+}+Mn) and (Mg–Li)–(Fe^{tot}+Mn+Ti–Al^{VI}) diagrams, whereas biotites from the phyllic zone plot in the Mg-biotite field (Fig. 3c–d). As in the Lakange and Qulong deposits, biotites from other porphyry copper polymetallic deposits have the characteristics of magnesium-rich (Mg-biotite or phlogopite), e.g., the Casino, Dalli, Miduk, Sarcheshmeh, Kahang, Darreh-Zar, and Jiama porphyry copper polymetallic deposits (Selby et al., 2000; Ayati et al.,

Table 1 Representative electron-microprobe analyses of biotites in the Lakange deposit (some data taken from Tang et al., 2017)

Biotite type	Magmatic biotites			Biotites from potassic zone			Biotites from phyllic zone		
n	15			15			14		
	Minimum	Maximum	Average	Minimum	Maximum	Average	Minimum	Maximum	Average
Oxide composition (wt%)									
SiO_2	36.26	39.53	37.97	37.98	41.22	40.00	34.99	40.58	38.30
Al_2O_3	12.45	15.33	13.63	11.47	14.57	13.33	12.91	16.45	14.57
TiO_2	2.84	3.52	3.26	1.12	2.64	2.02	0.78	2.74	2.13
FeO*	11.09	16.39	14.62	7.34	12.09	9.73	7.59	17.12	12.81
MnO	0.09	0.35	0.16	0.06	0.67	0.17	0.05	0.19	0.13
MgO	12.49	15.26	14.18	17.00	19.42	18.01	12.06	18.88	14.78
BaO	0.09	1.09	0.31	0.00	0.11	0.04	0.00	0.72	0.08
CaO	0.00	0.06	0.02	0.00	0.09	0.03	0.00	0.07	0.02
Na_2O	0.12	0.26	0.18	0.10	0.23	0.15	0.02	0.25	0.14
K_2O	8.87	9.83	9.41	8.88	10.25	9.52	8.41	9.87	9.17
F	0.71	1.91	1.09	0.85	2.90	1.88	0.79	2.46	1.42
Cl	0.01	0.07	0.05	0.01	0.09	0.03	0.01	0.10	0.04
CuO	0.00	0.07	0.02	0.00	0.09	0.02	0.00	0.19	0.03
O=F,Cl	0.32	0.81	0.47	0.37	1.23	0.80	0.34	1.04	0.61
H_2O_{calc}	3.04	3.58	3.39	2.61	3.52	3.07	2.83	3.56	3.21
$Total_{calc}$	97.39	100.48	98.74	93.76	100.80	98.81	95.05	99.98	97.46
Number of ion on the basis of 22 atoms of oxygen									
Si	5.655	5.989	5.802	5.839	6.171	6.036	5.521	6.112	5.883
$Al^{(IV)}$	2.011	2.345	2.198	1.829	2.161	1.964	1.888	2.479	2.118
T Site	8	8	8	8	8	8	8	8	8
$Al^{(VI)}$	0.068	0.551	0.256	0.247	0.722	0.406	0.301	0.739	0.521
Ti	0.320	0.407	0.375	0.127	0.309	0.230	0.088	0.325	0.247
Fe^{3+}	0.250	0.344	0.297	0.179	0.266	0.225	0.203	0.352	0.277
Mn	0.012	0.045	0.020	0.007	0.087	0.022	0.006	0.025	0.017
Mg	2.857	3.495	3.230	3.867	4.307	4.050	2.812	4.190	3.382
Fe^{2+}	1.118	1.760	1.572	0.725	1.250	1.004	0.751	1.890	1.374
O Site	5.559	5.869	5.751	5.812	6.000	5.937	5.614	6.000	5.818
Na	0.034	0.078	0.054	0.030	0.067	0.045	0.005	0.073	0.043
K	1.723	1.930	1.835	1.707	1.936	1.833	1.657	1.958	1.798
Ca	0.000	0.009	0.003	0.000	0.014	0.005	0.000	0.012	0.004
Ba	0.000	0.010	0.001	0.000	0.003	0.000	0.000	0.000	0.000
A Site	1.767	1.995	1.891	1.761	1.978	1.883	1.673	2.033	1.845
F	0.344	0.917	0.525	0.409	1.376	0.896	0.378	1.165	0.691
Cl	0.003	0.019	0.013	0.003	0.022	0.008	0.002	0.027	0.011
OH	3.074	3.637	3.462	2.617	3.582	3.096	2.830	3.616	3.298
X_{Mg}	0.512	0.598	0.561	0.654	0.719	0.682	0.501	0.698	0.581
X_{Fe}	0.356	0.448	0.397	0.250	0.313	0.288	0.289	0.469	0.392
$\log(X_F/X_{OH})$	−1.024	−0.525	−0.834	−0.942	−0.279	−0.550	−0.981	−0.386	−0.694
$\log(X_{Cl}/X_{OH})$	−3.021	−2.261	−2.450	−3.009	−2.109	−2.674	−3.145	−2.105	−2.581
$\log(X_F/X_{Cl})$	1.255	2.100	1.616	1.682	2.486	2.124	1.293	2.541	1.887
IV(F)	1.579	1.987	1.852	1.462	2.085	1.724	1.581	2.013	1.741
IV(Cl)	−3.847	−3.095	−3.644	−4.286	−3.327	−3.653	−4.051	−3.143	−3.550
IV(F/Cl)	5.047	5.727	5.496	5.034	5.934	5.377	4.893	5.773	5.291
$\log(fH_2O/fHF)$	3.947	4.414	4.253	5.415	6.056	5.686	5.549	6.471	6.079
$\log(fH_2O/fHCl)$	4.392	5.166	4.589	5.119	5.995	5.654	5.189	6.109	5.681
$\log(fHF/fHCl)$	−0.583	0.186	−0.281	−1.692	−0.814	−1.164	−2.006	−0.697	−1.447
T	706	746	727	396	453	422	278	425	335

X_{Mg} = Mg/(Mg + Fe, X_{Fe} = (Fe + Al^{VI})/(Fe + Mg + Al^{VI}). Methods of fluorine IV(F), chlorine IV(Cl), and fluorine/chlorine IV(F/Cl) intercept values are from Munoz (1984). The fugacity ratios of log (fH_2O)/(fHF), log (fH_2O)/($fHCl$), and log (fHF)/($fHCl$) are calculated using the equations by Munoz (1992). Calculating method for magmatic biotite Ti in biotite geothermometer is from Henry et al. (1974), Calculating method for hydrothermal biotite geothermometer is from Beane (1974).Note: FeO*, total iron as FeO.

2008; Boomeri et al., 2009; 2010; Afshooni et al., 2013; Parsapoor et al., 2015; Tang et al., 2016). Mg-rich biotite is likely to be a typical characteristic of porphyry copper polymetallic deposits.

3 Geothermometry

The concentration of Ti in biotite is very sensitive to temperature and oxygen fugacity, making it possible to use biotite to obtain reliable temperature estimates in igneous and metamorphic rocks (Robert, 1976; Patino Douce, 1993). Henry et al. (2005) calibrated empirically the relation between Ti content, temperature and Mg/(Mg+Fe) value (Fig. 4) using an extensive natural biotite data set (529 samples) from western Maine and south-central Massachusetts. The temperatures of biotite can be determined either by plotting biotite Ti and Mg/(Mg+Fe) values on Fig. 4 or by calculating temperatures directly from Ep (1). The temperatures of magmatic biotites from the Lakange and Qulong deposits, calculated by the empirical Ti-in-biotite geothermometer of Henry (2005), lie within the range of 706°C to 746°C (mean= 727°C) and 709°C to 779°C (mean =748°C) respectively.

$$T=\{[\ln(Ti)-a-c(X_{Mg})^3]/b\}^{0.333} \quad (1)$$

Table 2 Representative electron-microprobe analyses of biotites in the Qulong deposit

Biotite type	Magmatic biotite			Biotite from potassic zone			Biotite from phyllic zone		
n	16			16			10		
	Minimum	Maximum	Average	Minimum	Maximum	Average	Minimum	Maximum	Average
Oxide composition (wt%)									
SiO_2	37.96	40.60	39.22	36.94	42.03	40.08	36.86	39.86	38.45
Al_2O_3	12.51	15.57	14.30	13.49	19.08	15.02	12.52	20.53	15.84
TiO_2	2.68	9.24	3.76	1.54	2.98	2.31	1.64	2.55	1.99
FeO*	7.64	17.28	11.04	5.35	11.62	8.7	8.81	16.34	12.89
MnO	0.08	0.32	0.16	0.05	0.34	0.13	0.10	0.23	0.14
MgO	13.65	19.26	16.89	16.98	21.42	18.6	14.47	16.99	15.7
BaO	0.22	0.66	0.49	0.00	0.07	0.03	0.01	0.13	0.05
CaO	0.00	0.19	0.03	0.00	0.12	0.04	0.01	0.10	0.03
Na_2O	0.14	0.24	0.18	0.11	0.19	0.15	0.09	0.25	0.16
K_2O	8.57	9.41	9.04	8.07	10.32	9.21	8.7	9.76	9.36
F	0.28	1.17	0.83	0.70	1.45	1.06	0.35	0.93	0.6
Cl	0.05	0.13	0.07	0.03	0.08	0.05	0.03	0.13	0.07
CuO	0.00	0.35	0.04	0.00	0.06	0.01	0.00	0.05	0.02
O=F,Cl	0.15	0.50	0.37	0.30	0.62	0.46	0.17	0.40	0.27
H_2O_{calc}	3.48	3.81	3.66	3.4	3.73	3.58	3.58	3.86	3.73
$Total_{calc}$	98.58	102.18	100.07	96.82	101.84	99.44	97.26	100.83	99.32
Number of ion on the basis of 22 atoms of oxygen									
Si	5.46	5.93	5.77	5.45	6.01	5.86	5.48	5.88	5.71
$Al^{(IV)}$	2.07	2.39	2.22	1.99	2.55	2.14	2.12	2.52	2.29
T Site	8.00	8.00	8.00	8.00	8.00	8.00	8.00	8.00	8.00
$Al^{(VI)}$	0.00	0.50	0.26	0.28	0.76	0.45	0.06	1.08	0.47
Ti	0.30	0.99	0.42	0.17	0.33	0.25	0.18	0.29	0.22
Fe^{3+}	0.20	0.32	0.25	0.14	0.26	0.21	0.21	0.32	0.26
Mn	0.01	0.04	0.02	0.01	0.04	0.02	0.01	0.03	0.02
Mg	3.07	4.18	3.70	3.71	4.53	4.06	3.21	3.78	3.47
Fe^{2+}	0.71	1.86	1.11	0.50	1.18	0.85	0.87	1.77	1.35
O Site	5.63	5.86	5.76	5.73	5.93	5.84	5.70	5.90	5.79
Na	0.04	0.07	0.05	0.03	0.05	0.04	0.03	0.07	0.05
K	1.62	1.81	1.70	1.48	1.94	1.72	1.65	1.88	1.77
Ca	0.00	0.03	0.00	0.00	0.02	0.01	0.00	0.02	0.00
Ba	0.00	0.02	0.00	0.00	0.00	0.00	0.00	0.00	0.00
A Site	1.67	1.86	1.75	1.56	1.98	1.77	1.71	1.91	1.83
F	0.13	0.55	0.39	0.32	0.65	0.49	0.16	0.44	0.28
Cl	0.01	0.03	0.02	0.01	0.02	0.01	0.01	0.03	0.02
OH	3.44	3.84	3.60	3.34	3.67	3.5	3.56	3.81	3.70
X_{Mg}	0.54	0.72	0.64	0.64	0.77	0.69	0.55	0.64	0.60
X_{Fe}	0.19	0.42	0.30	0.2	0.32	0.27	0.34	0.43	0.37
$\log(X_F/X_{OH})$	−1.47	−0.80	−1.00	−1.05	−0.71	−0.86	−1.37	−0.91	−1.14
$\log(X_{Cl}/X_{OH})$	−2.46	−2.05	−2.32	−2.77	−2.25	−2.46	−2.64	−2.06	−2.33
$\log(X_F/X_{Cl})$	0.59	1.67	1.32	1.25	1.95	1.6	0.83	1.73	1.19
IV(F)	1.93	2.46	2.11	1.85	2.22	2.04	1.94	2.36	2.19
IV(Cl)	−4.06	−3.85	−3.93	−4.18	−3.61	−3.88	−4.09	−3.5	−3.84
IV(F/Cl)	5.79	6.45	6.04	5.76	6.23	5.92	5.44	6.38	6.03
$\log(fH_2O/fHF)$	4.07	4.91	4.41	5.36	6.07	5.77	6.26	6.87	6.52
$\log(fH_2O/fHCl)$	4.18	4.64	4.45	4.99	5.69	5.33	5.15	5.82	5.43
$\log(fHF/fHCl)$	−1.31	−0.28	−0.64	−1.93	−1.06	−1.52	−2.55	−1.73	−2.17
T	709	779	748	381	495	429	314	361	339

X_{Mg}=Mg/(Mg+Fe, X_{Fe}=(Fe+Al^{VI})/(Fe+Mg+Al^{VI}). Methods of fluorine IV(F), chlorine IV(Cl), and fluorine/chlorine IV(F/Cl) intercept values are from Munoz (1984). The fugacity ratios of log (fH_2O)/(fHF), log (fH_2O)/($fHCl$), and log (fHF)/($fHCl$) are calculated using the equations by Munoz (1992). Calculating method for magmatic biotite Ti in biotite geothermometer is from Henry et al. (1974), Calculating method for hydrothermal biotite geothermometer is from Beane (1974). Note: FeO*, total iron as FeO.

where T is temperature in °C, Ti is the apfu normalized to 22 O atoms, X_{Mg} is Mg/(Mg+Fe), a=2.3594, b=4.6482e−9, and c=−1.7283. This expression is valid in the range X_{Mg}=0.275–1.000, Ti=0.04–0.60 apfu and T= 480–800°C.

Compositional variation in biotite has been applied to geothermometry and oxygen geobarometry at high temperatures (Wones and Eugster, 1965). Such results have not as yet been formally extended to hydrothermal silicate-sulfide system at near-atmospheric pressures and temperatures on the order of 100°C to 300°C. Biotite geothermometer (T–X_{phl}) proposed by Beane (1974) for hydrothermal biotites in the potassic alteration zone of the North American porphyry copper deposits including Santa Rita, Ray, Safford, Bingham, Hanover and Galore Creek (Fig. 5), where hydrothermal biotites coexist with magnetite and K-feldspar assemblage. The hydrothermal biotite geothermometer (T–X_{phl}) is applied to biotites from the potassic and phyllic alteration zones of Dalli and Kahang porphyry copper deposits (Fig. 5). Calculated temperatures for biotites from the phyllic alteration zone lie within the range of 278°C to 352°C with a mean value of 316°C, while bitoties from the potassic alteration zone is characterized by the higher temperatures ranging from 388°C to 453°C (mean=420°C) in the Lakange porphyry Cu–Mo deposit (Fig. 5). Calculated temperatures for

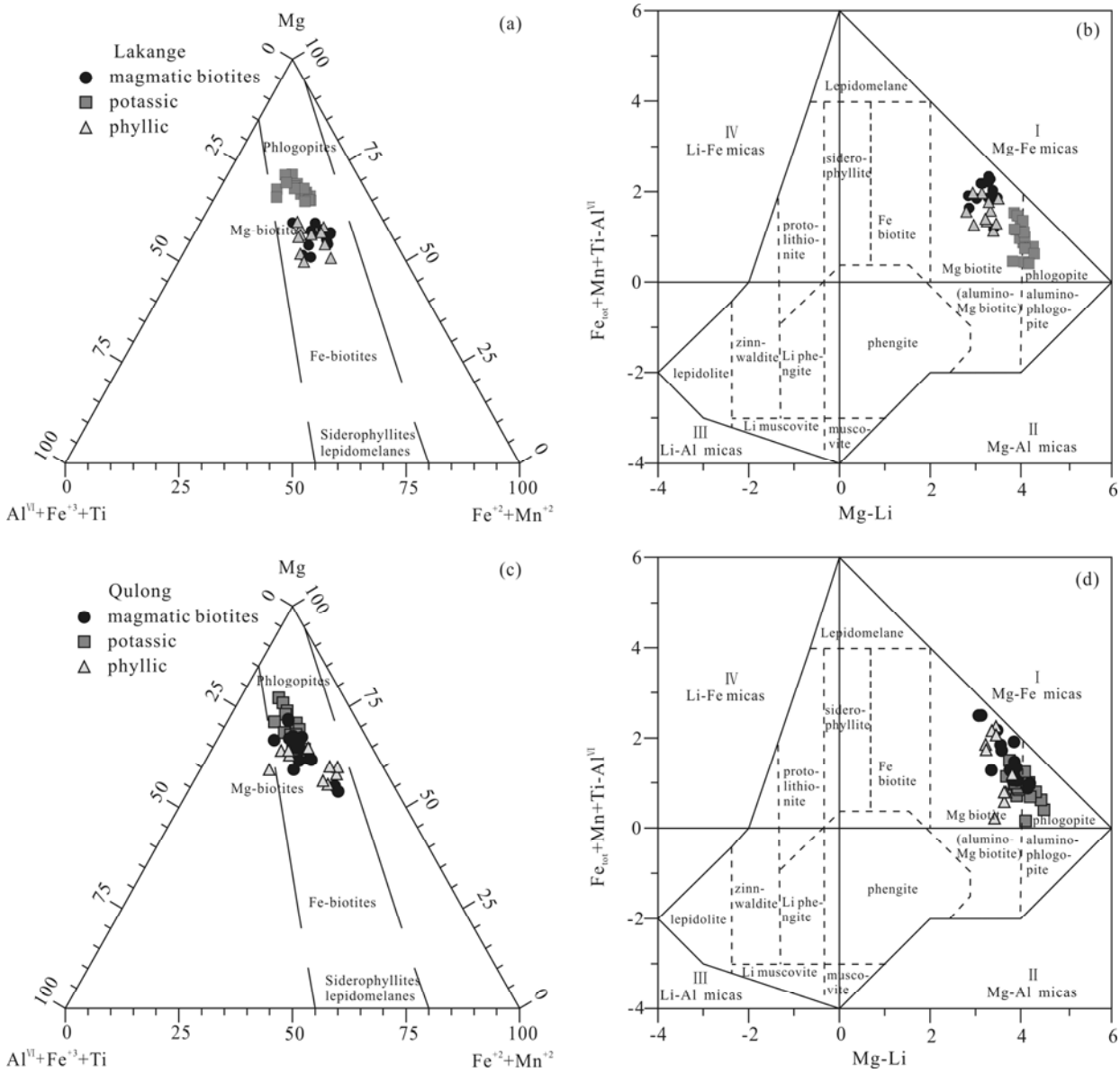


Fig. 3. Chemical composition of biotites from the Lakange and Qulong deposits on classification diagrams (a and c after Foster, 1960; b, and d after Tischendorf et al., 1997)

biotites from the phyllic alteration lie within the range of 314°C to 361°C with a mean value of 339°C, while the potassic alteration zone is characterized by the higher temperatures ranging from 381°C to 495°C (mean=428°C) in the Qulong porphyry Cu deposit (Fig. 5).

4 Geobarometry

Uchida et al. (2007) found a positive correlation between ^{T}Al content in biotite and the solidification pressure of the granitic rocks, and used the ^{T}Al content in biotite to estimate the solidification pressure (P) of the granitic rocks (equation 2).

$$P(kb)=3.03\times{}^{T}Al-6.53\ (\pm 0.33) \quad (2)$$

where ^{T}Al designates the total Al content in biotite on the basis O=22.

The ^{T}Al-in-biotite geobarometer has been used to estimate the solidification pressure and depth of emplacement of the granitic rocks as well as ore-forming potential. By using the biotite geobarometer of Uchida et al. (2007), the solidification pressures of the Ge'erkuohe porphyry granitoid, western Qinling, are estimated as 131–181 MPa, corresponding to solidification depth of 5.0−7.1 km (Guo et al., 2015); the solidification pressures of the Ziyunshan granite, central Jiangxi, are estimated as 253–322 MPa, corresponding to solidification depth of 10–12 km (Tang et al., 2015); the solidification pressures of the Yanshanian granitic pluton in Luanchuan ore concentration area are estimated as 38–115 MPa, corresponding to solidification depth of 1.4–4.4 km (Xu et al., 2015); the solidification pressures of the Huangbeiling granite are estimated as 93–14 MPa, corresponding to solidification depth of 3.4–0.5 km (Wu et al., 2015); the solidification pressures of the Guyong granite in western

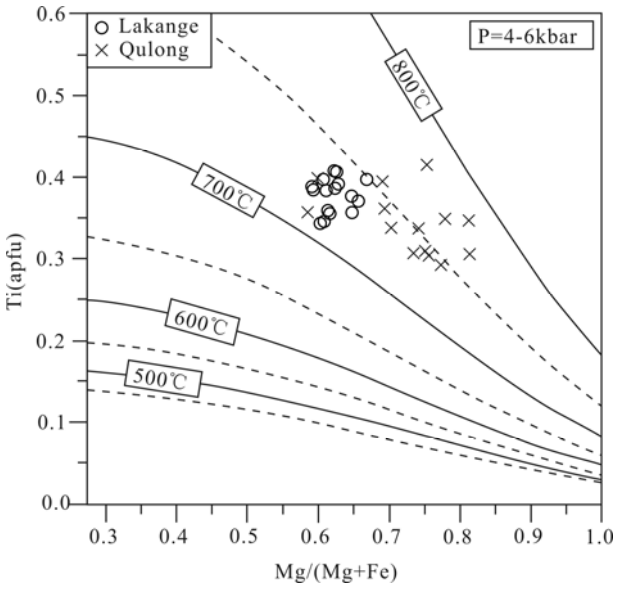


Fig. 4. Temperature isotherms (°C) calculated from the surface-fit equation on Ti vs. Mg/(Mg+Fe) diagram (after Henry et al., 2005).

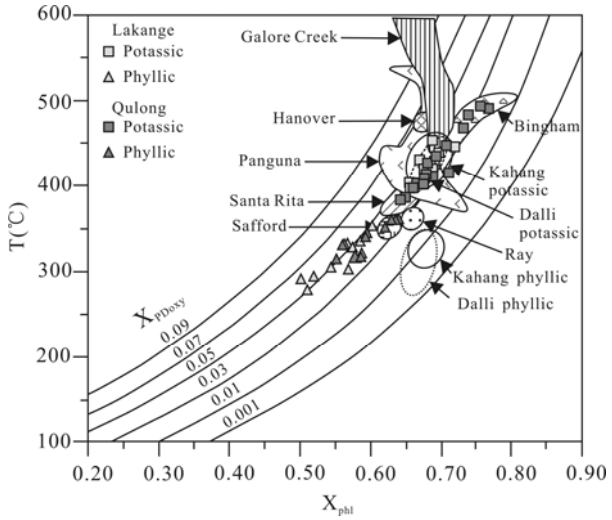


Fig. 5. Compositions of biotites from the Lakange and Qulong deposits on X_{phl} vs. Temperature (°C) diagram (modified from Beane, 1974; Ayati et al., 2008; Afshooni et al., 2013).

The Galore Creek, Santa Rita, Safford, Ray, and Hanover porphyry copper deposits are taken from Beane (1974); The Panguna, Bingham, Dalli, and Kahang porphyry copper deposits are taken from Ford (1978) and Laner et al. (1978), Ayati et al. (2008), Afshooni et al. (2013) respectively.

Yunnan are estimated as 67–120 MPa, corresponding to solidification depth of 3.4–0.5 km (Chen et al., 2015); and the solidification pressures of the Wushan granodiorite in Jiangxi Province are estimated as 86–103 MPa, corresponding to solidification depth of 2.84–3.39 km favoring the formation of the Wushan copper deposit (Dong et al., 2011).

5 Oxygen Fugacity

Wones and Eugster (1965) proposed that X_{Mg} [X_{Mg}=Mg/(Mg+ Fe)] of biotite increases with higher oxygen and (or) sulfur fugacity in magma and fluids and found that, as oxygen fugacity increases in magmatic systems, the Fe^{3+}/Fe^{2+} ratio in the melt increases, leaving progressively less Fe^{2+} able to compete with Mg^{2+} for site occupancy in mafic minerals. Accordingly, as fO_2 increases, the X_{Mg} of mafic minerals will be increased. Therefore, high X_{Mg} in mafic minerals appears to be characteristic of high-fO_2 magmas. Wones et al. (1965) proposed that the Fe^{2+}–Fe^{3+}–Mg ternary of biotite is consistent with the oxygen buffers, i.e., quartz–fayalite–magnetite (QFM), nickel–nickel oxide (NNO), and hematite–magnetite (HM) (Fig. 6). The oxygen fugacity is widely used in studying granite and porphyry deposits (Loferski et al., 1995; Li et al., 2007a, 2007b; Liu et al., 2010; Chen et al., 2010, 2013; Zhang et al., 2011; Afshooni et al., 2013; Wu et al., 2015; Parsapoor et al., 2015; Tang et al., 2016; Zhang et al., 2016).

The composition of magmatic and hydrothermal biotites in the potassic and phyllic alteration zone from the Lakange porphyry Cu–Mo deposit and the Qulong porphyry Cu deposit falls on or above the NNO buffer in the Fe^{3+}–Fe^{2+}–Mg diagram of Wones and Eugster (1965), which show high oxygen fugacity. In the Lakange porphyry Cu–Mo deposit, the X_{Mg} of magmatic biotites is 0.51–0.60 (mean=0.56), the X_{Mg} of hydrothermal biotites in the potassic alteration zone is 0.65–0.72 (mean=0.68), and the X_{Mg} of hydrothermal biotites in the phyllic alteration zone is 0.50–0.70 (mean=0.58). The above suggests that the X_{Mg} of hydrothermal biotites in the potassic alteration zone is higher than that of magmatic biotites and hydrothermal biotites in the phyllic alteration zone, and the X_{Mg} of hydrothermal biotites in the phyllic alteration zone is higher than that of magmatic biotites. In addition, the Fe^{3+}/Fe^{2+} of hydrothermal biotites in the potassic alteration zone is 0.19–0.24 (mean=0.22), the Fe^{3+}/Fe^{2+} of hydrothermal biotites in the phyllic alteration zone is 0.15–0.22 (mean=0.18), and the Fe^{3+}/Fe^{2+} of magmatic biotites is 0.13–0.21 (mean=0.17). Clearly, Fe^{3+}/Fe^{2+} gradually decrease from hydrothermal biotites in the potassic alteration zone to hydrothermal biotites in the phyllic alteration zone to magmatic biotites. Therefore, the oxygen fugacity gradually increases from magmatic biotites to hydrothermal biotites, whereas decreases from hydrothermal biotites in the potassic alteration zone to hydrothermal biotites in the phyllic alteration zone in the Lakange porphyry Cu–Mo deposit. In the Qulong porphyry Cu deposit, the X_{Mg} of magmatic biotites is 0.54–0.72 (mean=0.64), the X_{Mg} of hydrothermal biotites in the potassic alteration zone is 0.64–0.77 (mean=0.69), and the X_{Mg} of hydrothermal biotites in the phyllic alteration zone is 0.55–0.64 (mean=0.60). The above suggest that the X_{Mg} of hydrothermal biotites in the potassic alteration zone is higher than that of magmatic biotites and hydrothermal biotites in the phyllic alteration zone, and the X_{Mg} of magmatic biotites is higher than hydrothermal biotites in the phyllic alteration zone. In addition, the Fe^{3+}/Fe^{2+} of hydrothermal biotites in the potassic alteration zone is 0.22–0.28 (mean=0.25), the Fe^{3+}/Fe^{2+} of hydrothermal biotites in the phyllic alteration zone is 0.15–0.26 (mean=0.20), and the Fe^{3+}/Fe^{2+} of magmatic biotites

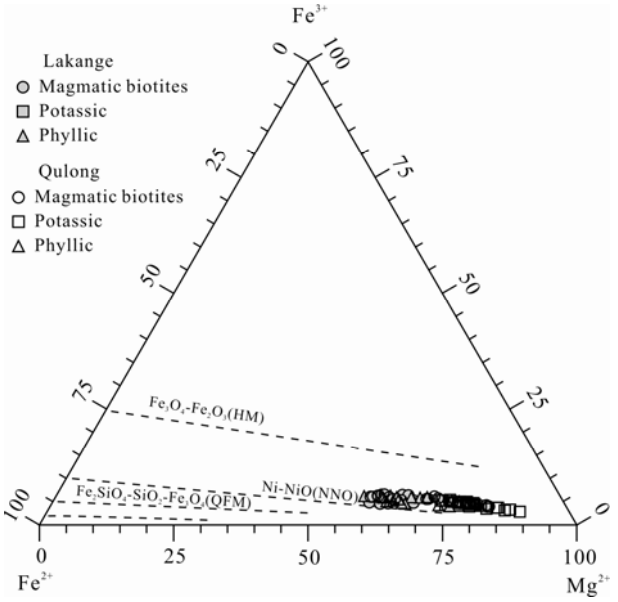


Fig. 6. Compositions of biotites from the Lakange and Qulong deposits on the Fe^{3+}–Fe^{2+}–Mg diagram (after Wones et al., 1965).

is 0.17–0.28 (mean=0.24). Apparently, Fe^{3+}/Fe^{2+} gradually decrease from hydrothermal biotites in the potassic alteration zone to magmatic biotites to hydrothermal biotites in the phyllic alteration zone. Therefore, the oxygen fugacity gradually increases from magmatic biotites to hydrothermal biotites in the potassic alteration zone, whereas decreases from hydrothermal biotites in the potassic alteration zone to hydrothermal biotites in the phyllic alteration zone in Qulong porphyry Cu deposit.

High oxygen fugacity (fO_2) is critical to the formation of porphyry and epithermal deposits because sulfur is dissolved in silicate melts as SO_4^{2-} and SO_2 in silicate melts under the condition of high fO_2. Forming supersaturated sulfide in magma is not easy in high fO_2 conditions so that the chalcophile element Cu is concentrated in the melt phase in the process of magmatic-hydrothermal evolution and eventually into the fluid phase, which is advantageous to Cu mineralization (Xiong et al., 2001; Bi et al., 2009; Li et al., 2008). Molybdenum mineralization is associated with oxidized felsic granites (Mengason et al., 2011). It is generally believed that the ore fluids responsible for porphyry Cu (Mo–Au) mineralization are relatively oxidized, with oxygen fugacity ranging between the NNO and HM buffers (Burnham et al., 1980; Afshooni et al., 2013). For example, the Deboullie pluton that is associated with porphyry Cu–Mo mineralization crystallized at the NNO buffer (Loferski et al., 1995), the Kahang porphyry Cu deposit formed from the HM to NNO buffer (Afshooni et al., 2013), and the Darreh-Zar porphyry Cu deposit formed from the HM to NNO buffer (Parsapoor et al., 2015). The Lakange porphyry Cu–Mo and Qulong porphyry Cu deposits formed from high oxygen fugacity conditions above the NNO. The change in temperature and oxygen fugacity may favor the precipitation of copper and molybdenum.

6 Petrogenesis and Tectonic Setting

Biotite mineral chemistry can be used to decipher tectono-magmatic processes and granite petrogenesis (Dodge et al., 1969; Barrière et al., 1979; Neiva, 1981; Speer, 1981; Ague et al., 1988; Finch et al., 1995), for it reflects geothermometry, oxygen fugacity, geobarometer and tectonic setting (Nachit et al., 1985; Lalonde et al. 1993; Burkhard, 1993; Abdel-Rahman, 1994; Zhou, 1986).

Biotite is widespread occurrence in all types of granite and granitoid. Biotite can by virtue of their crystal structure accommodate most of the common elements present in granitic magmas (Shabani et al., 2003). The following features make biotite a valuable probe of magma composition: 1) It is the most important reservoir of any excess aluminium in granites that do not have important amounts of garnet, cordierite or Al_2SiO_5 polymorphs; therefore it directly reflects the peraluminosity of the host magma in such rocks, and 2) it is the most readily available indicator of oxidation state (Shabani et al., 2003). The aluminum saturation index (ASI) of biotite and host rock is positively correlation in granitic rocks that biotite is the most common mineralogical sink for excess aluminum (De Albuquerque, 1973; Speer, 1981; Lalonde a et al., 1993).

Biotite is Fe-rich in A-type granites, Mg-rich in I-type granites, and Al-rich in S-type granites (Abdel-Rahman, 1994; Shabani et al., 2003). The $Mg^{\#}$ and oxidation index of biotite can be used to classify granites into I- and S-types. Biotite in I-type granites has higher $Mg^{\#}$ (0.384–0.626) and oxidation index (0.252–0.121) than in S-type granites (Xu et al., 1986). A-type, ca1c-alkaline I-type and S-type granites can be distinguished by using the Fe/(Fe + Mg) –F diagram of Dahlquist et al. (2010). I-type, S-type and shoshonitic granites can be distinguished by using the Al^{IV}–$Fe^{2+}/(Fe^{2+}+Mg)$ diagram of Jiang et al. (2002).

The MgO–FeO_{tot}–Al_2O_3 diagram of De Albuquerque (1973) can be used to distinguish between biotites coexisting with amphibole, unaccompanied by other ferro-magnesian minerals, coexisting with muscovite and coexisting with aluminosilicates (sillimanite or andalusite). The Al–Mg diagram of Nachit et al. (1985) classifies granites into peraluminous, calc-alkaline, subalkaline subalkaline, and alkaline-parlkaline. A biotite IV(F) systematics show that calcalkaline biotites have high IV(F) (1.1 to 2.8, mean=2.19), high-K calcalkaline biotites display middle IV(F) (0.75 to 1.7, mean=1.42), high-silica alkaline display low IV(F) (−0.8 to 1.9, mean=0.56), and peraluminous biotites show a wide range of IV(F) (0.2 to 2.3, mean=1.5) (Sallet, 2000). Czamanske et al. (1981) and Lalonde et al. (1993) suggested that the biotite compositions define a continuum from the magnetite-series granites on Fe/(Fe+Mg)–Al diagram, with the most Mg-rich and Al-poor biotite, to the ilmenite-series with increasing Fe- and Al-contents. The biotite compositions from the magnetite-series and ilmenite-series granites in Maherabad, Dehnow, Gheshlagh, Khajehmourad and Najmabad on TiO_2–Al_2O_3 diagram show that biotites in magnetite-series granites have high TiO_2 and low Al_2O_3, whereas biotites in ilmenite-series

granites have low TiO_2 and high Al_2O_3 (Karimpour, 2011).

Zhou (1986) collected biotite data from 15 regions around the world and pointed out that the $w(\sum FeO)/w(\sum FeO + MgO)$–$w(MgO)$ diagram of biotite can be used to discriminate sources of granite, that is, crust, crust-mantle and mantle. Abdel-Rahman (1994) studied 325 magmatic biotites chemistry from different tectonic environments and found that the $MgO–FeO_{tot}–Al_2O_3$ diagram of biotite can be used to distinguish the tectonic environment of host magmas, that is, anorogenic alkaline suites, calc-alkaline orogenic suites and peraluminous suites including S-type granites. Ague et al. (1988) pointed out that the $\log(X_F/X_{OH})$–$\log(X_{Mg}/X_{Fe})$ of biotite shows the degree of contamination of I-type granite (the term "contamination" is used here in a broad sense to refer to interactions of mafic "I-type" magmas derived from the upper mantle, deep crust, or subducted slabs with continental crustal source components), including I-SC (strongly contaminated I-type), I-MC (moderately contaminated I-type), I-WC (weakly contaminated I-type) and I-SCR (strongly contaminated and reduced I-type).

Hu et al. (2006) studied biotites in the Longwo and Baishigang plutons in Guangdong province and concluded that the composition of biotite can be used to trace the magmatic differentiation. With increasing magmatic differentiation, the Rb content in biotite increases, and the Ba content decreases; consequently, Rb/Ba increases. Smith et al. (2011) found that biotite in the Younger Toba Tuff has lower FeO/MgO (2.1–2.6) than in the products of older eruptions (2.8–3.7).

Biotite composition can help in understanding petrogenesis and tectonic setting of granite but needs to be combined with other geological data, such as major or trace element, isotope and regional geology (Abdel-Rahman, 1994; Shabani et al., 2003; Hu et al., 2006). The magmatic biotites from the Lakange and Qulong porphyry deposits plot on the calc-alkaline orogenic suite on the ternary $MgO–FeO_{tot}–Al_2O_3$ diagram (Abdel-Rahman, 1994) (Fig. 7), consistent with the geochemical work of Leng et al. (2016a), Gao et al. (2006) and Wang et al. (2006). The magmatic biotites from the Lakange porphyry deposit plot on the crust-mantle field on $w(SFeO)/w(SFeO+MgO)$–$w(MgO)$ diagram (Zhou, 1986) (Fig. 8), agreement with zircon Hf isotope (Leng et al., 2016a, 2016b). The magmatic biotites from Qulong porphyry deposit plot on the crust-mantle and mantle fields on the $w(\sum FeO)/w(\sum FeO + MgO)$–$w(MgO)$ diagram (Zhou, 1986) (Fig. 8), consistent with zircon Hf isotope (Yang et al., 2008).

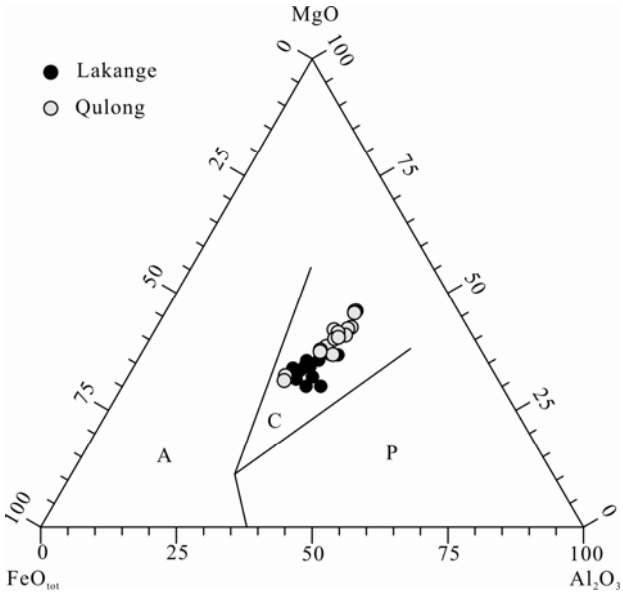


Fig. 7. Compositions of biotites from the Lakange and Qulong deposits on $MgO–FeO_{tot}–Al_2O_3$ diagram (after Abdel-Rahman, 1994).
A–anorogenic alkaline suites; C–calc-alkaline orogenic suites; P–peraluminous suites (including S-type).

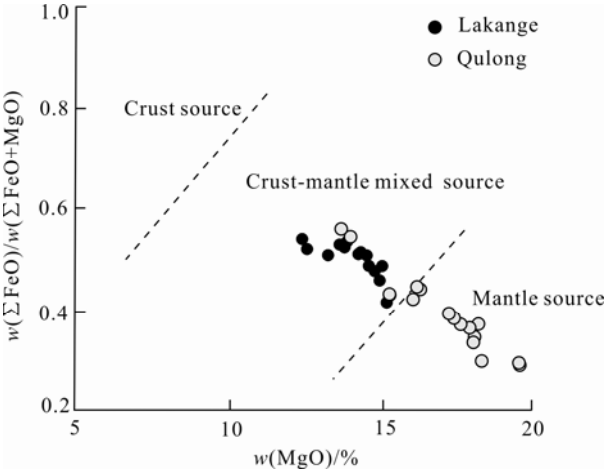


Fig. 8. Compositions of biotites from the Lakange and Qulong deposits on $w(\Sigma FeO)/w(\Sigma FeO+MgO)$–$w(MgO)$ diagram (after Zhou, 1986).

7 Halogen Chemistry

7.1 Halogen content

Between 70% and 90% of fluorine in muscovite- and fluorite-free granitoid rocks is contained in biotite, with the remainder in apatite, amphibole and titanite (Grabezkev et al., 1979; Speer, 1984; Zhang et al., 2016). The F and Cl exist in biotite crystalline lattice by F=OH and Cl=OH exchange, and the Cl content of biotite is considerably less than the F content, because the ionic crystal radius of Cl^- in biotite is 1.81Å, which is significantly larger than either F^-(1.31 Å) or OH^- (1.38 Å) so that Cl=OH exchange less than F=OH exchange (Munoz, 1984). So, although the Cl content in biotite is less, very rich in magma or fluids associated with biotite. The extent of halogen replacement of hydroxyl in biotite is governed by its Mg/Fe ratio, biotites with high Mg/Fe ratios tend to incorporate more F, and low Mg/Fe biotites contain more Cl, as noted by Munoz (1984) in experiment. This correlation is caused by the crystal-chemical effect known as "F–Fe avoidance" and "Mg–Cl avoidance" (Munoz, 1984).

The composition of biotites from the phyllic alteration zone in the Kahang and Dalli porphyry Cu deposits, Deboullie pluton, Midukhe and Sarcheshmeh porphyry Cu deposits is consistent with the "Fe–F" and "Mg–Cl"

avoidance principles (Afshooni et al., 2013; Ayati et al., 2008; Loferski et al., 1995; Boomeri et al., 2009; Boomeri et al., 2010). However, the composition of biotites from Darreh-Zar porphyry Cu deposit, the potassic alteration zone in the Kahang and Dalli porphyry Cu deposits and Casino porphyry Cu-Au-Mo deposit is not consistent with the "Fe–F" and "Mg–Cl" avoidance principles (Parsapoor et al., 2015; Afshooni et al., 2013; Ayati et al., 2008; Selby et al., 2000). The F content of the Lakange magmatic and hydrothermal biotites in the phyllic alteration zone correlates positively with the mole fraction of Mg (X_{Mg}) and is consistent with the "Fe–F" avoidance principle, whereas the opposite is observed for the hydrothermal biotites in the potassic alteration zones (Fig. 9a). The Cl content of the Lakange magmatic and hydrothermal biotites in the potassic and phyllic alteration zones does not correlate negatively with the mole fraction of Mg (X_{Mg}) and is not consistent with the "Mg–Cl" avoidance principle (Fig. 9b). The F content of the Qulong magmatic and hydrothermal biotites in the phyllic alteration zones correlates positively with the mole fraction of Mg (X_{Mg}) and is consistent with the "Fe–F" avoidance principle, whereas the opposite is observed for the hydrothermal biotites in the potassic alteration zones (Fig. 9a). The Cl content of the Qulong magmatic biotites correlates negatively with the mole fraction of Mg (X_{Mg}) and is consistent with the "Mg–Cl" avoidance principle, whereas the opposite is observed in the hydrothermal biotite in the potassic and phyllic alteration zones (Fig. 9b). The weak correlation and uncorrelation suggests that biotite may have formed from different hydrothermal fluids.

Zhu and Sverjensky (1992) have shown that the composition of biotite formed under similar physicochemical conditions produces linear trends on log (X_F/X_{OH})–X_{Fe} and log(X_{Cl}/X_F)–X_{Fe} plots. The slopes of these trends are a function of temperature, and independent of pressure and fluid composition, whereas the intercept value is a function of all these parameters (Zhu and Sverjensky, 1992). Biotites from the potassic and phyllic zones in the Lakange porphyry Cu–Mo deposit have log(X_F/X_{OH}) values of −0.94 to −0.28 (mean=−0.55) and −0.98 to −0.39 (mean=−0.69), and log(X_{Cl}/X_{OH}) values of −3.01 to −2.11 (mean=−2.67) and −3.15 to −0.21 (mean=−2.58), respectively. Using the median temperatures of the Lakange potassic and phyllic alteration zones established from geothermometer (T-X_{phl}) of Beane (1974), that is, 420°C and 316°C, respectively, the slopes for log(X_{Cl}/X_{OH})–X_{Mg} and log(X_F/X_{OH})–X_{Fe} plots are derived from Eqs. 23 and 24 of Zhu and Sverjensky (1992). The slopes on the log(X_{Cl}/X_{OH})–X_{Mg} and the log(X_F/X_{OH})–X_{Fe} plots for biotites from the potassic zone are 2.03 and −1.68, respectively, and the values for biotites from the phyllic zone are −1.72 and −1.16 respectively (Fig. 10a−b). So the slopes y-intercepts of two types of hydrothermal biotites are obviously different (Fig. 10a−b). Biotites from the potassic and phyllic zones in the Qulong porphyry Cu deposit have log (X_F/X_{OH}) values of −1.05 to −0.71 (mean=−0.86) and

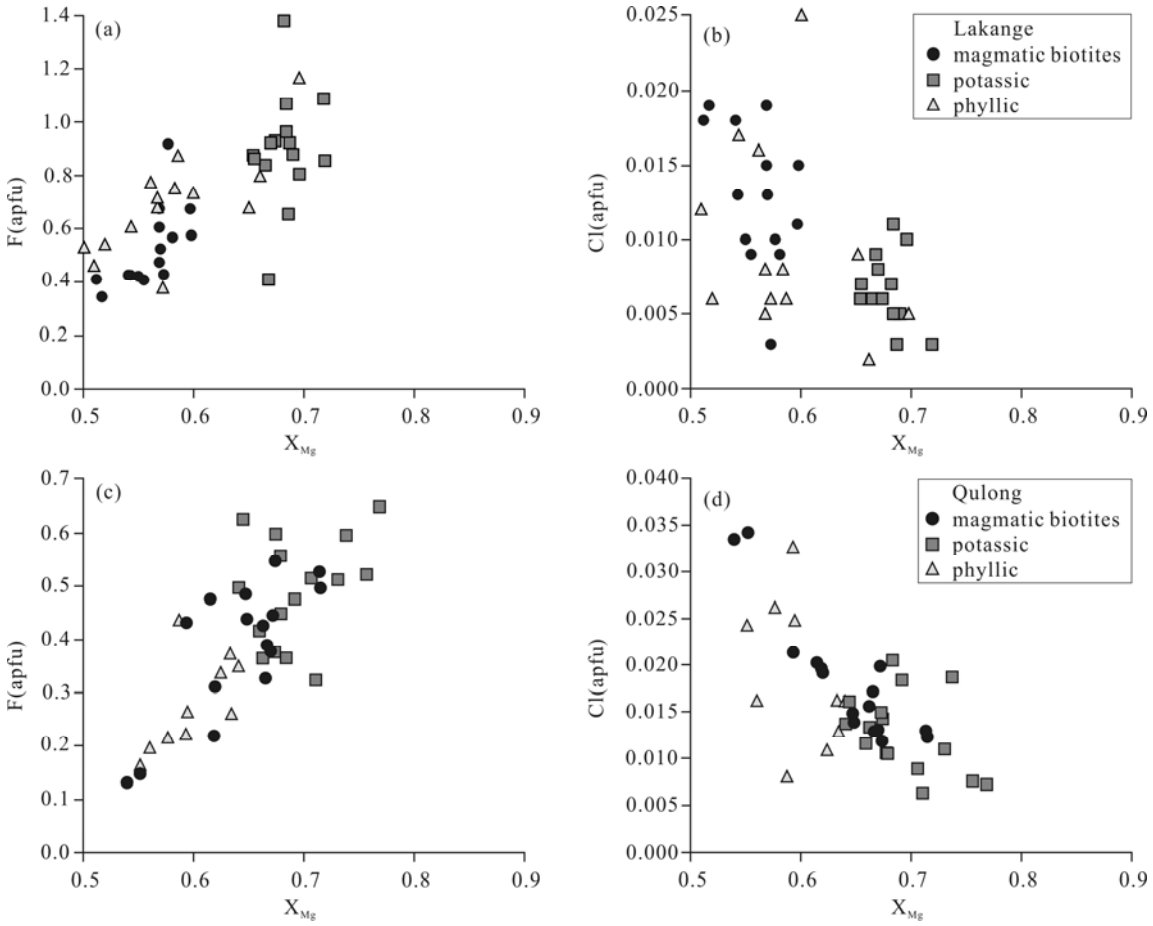


Fig. 9. Halogen compositions of biotites from the Lakange and Qulong deposits vs. X_{Mg}.

−1.37 to −0.91 (mean=−1.14), and $\log(X_{Cl}/X_{OH})$ values of −2.77 to −2.25 (mean=−2.46) and −2.64 to −2.06 (mean=−2.33), respectively. Using the median temperatures of the Qulong potassic and phyllic zones established from geothermometer ($T-X_{phl}$) of Beane (1974), that is, 428°C and 339°C, respectively, the slopes for the $\log(X_{Cl}/X_{OH})$–X_{Mg} and $\log(X_F/X_{OH})$–X_{Fe} plots are derived from Eqs. 23 and 24 of Zhu and Sverjensky (1992). The slopes on the $\log(X_{Cl}/X_{OH})$–X_{Mg} and the log (X_F/X_{OH})–X_{Fe} plots for biotites from the potassic zone are –1.18 and –0.61, respectively, and the values for biotite from the phyllic zone are –1.13 and 0.08, respectively (Fig. 10c–d). So the slopes and y-intercepts of $\log(X_{Cl}/X_{OH})$–X_{Mg} of two type of hydrothermal biotites are similar, but the slopes and y-intercepts of $\log(X_F/X_{OH})$–X_{Fe} are obviously different (Fig. 10c–d). Selby and Nesbitt (2000) attributed the similarity of intercepts and narrow scatter for the halogen content of biotite in the potassic and phyllic alteration zones from the Casino porphyry Cu–Au–Mo deposit, Yukon, Canada to the constant $\log(X_F/X_{OH})$ and $\log(X_{Cl}/X_{OH})$ values of hydrothermal fluid with broadly similar temperature conditions. Therefore, the log (X_F/X_{OH}) and $\log(X_{Cl}/X_{OH})$ values of hydrothermal biotites in the potassic and phyllic alteration zones from the Lakange porphyry Cu–Mo deposit and the Qulong porphyry Cu deposit are different, which suggests that the variable halogen content of hydrothermal fluids, and hydrothermal biotites chemistry records the change in fluid composition during the crystallization history of the magma.

Munoz (1984) pointed out that the fluorine intercept [IV (F)], the chlorine intercept [IV(Cl)], and the F/Cl intercept [IV(F/Cl)] values are important physicochemical parameters to describe the relative degree of F and Cl contents in biotite, which are all related to the fugacity ratios of f(HCl)/f(HF). These values are defined by Munoz (1984) as:

$IV(F)=1.5X_{Mg}+0.42X_{ann}+0.20X_{sid}-\log(X_F/X_{OH})$

$IV(Cl)=-5.01-1.93X_{Mg}-\log(X_{Cl}/X_{OH})$

$IV(F/Cl)=IV(F)-IV(Cl)$

The mole fractions of siderophyllite (X_{sid}) and of annite (X_{ann}) in biotite were obtained from following (Yavuz, 2003):

$X_{sid}=[(3-Si/Al)/1.75][1-X_{Mg}]$

$X_{ann}=1-(X_{Mg}-X_{sid})$.

Lower IV(F) values correspond to higher degree of fluorine enrichment. The IV(Cl) is always negative, so, the higher negative numbers indicate the higher degree of chlorine enrichment. Its subsequent, lower IV(F/Cl) values correspond to higher F/Cl ratio (Munoz, 1984; Yavuz, 2003a). The IV(F/Cl) value is independent of temperature, not affected by the uncertainties in the hydroxyl occupancy, and directly related to the f(HCl)/f(HF) of the fluid that equilibrated with the biotite, therefore, it gives more accurate results than either the IV(F) and IV(Cl) values (Munoz, 1984; van Middelaar and Keith, 1990; Yavuz, 2003).

Munoz (1984) evaluated IV(F), IV(Cl) and IV(F/Cl) in

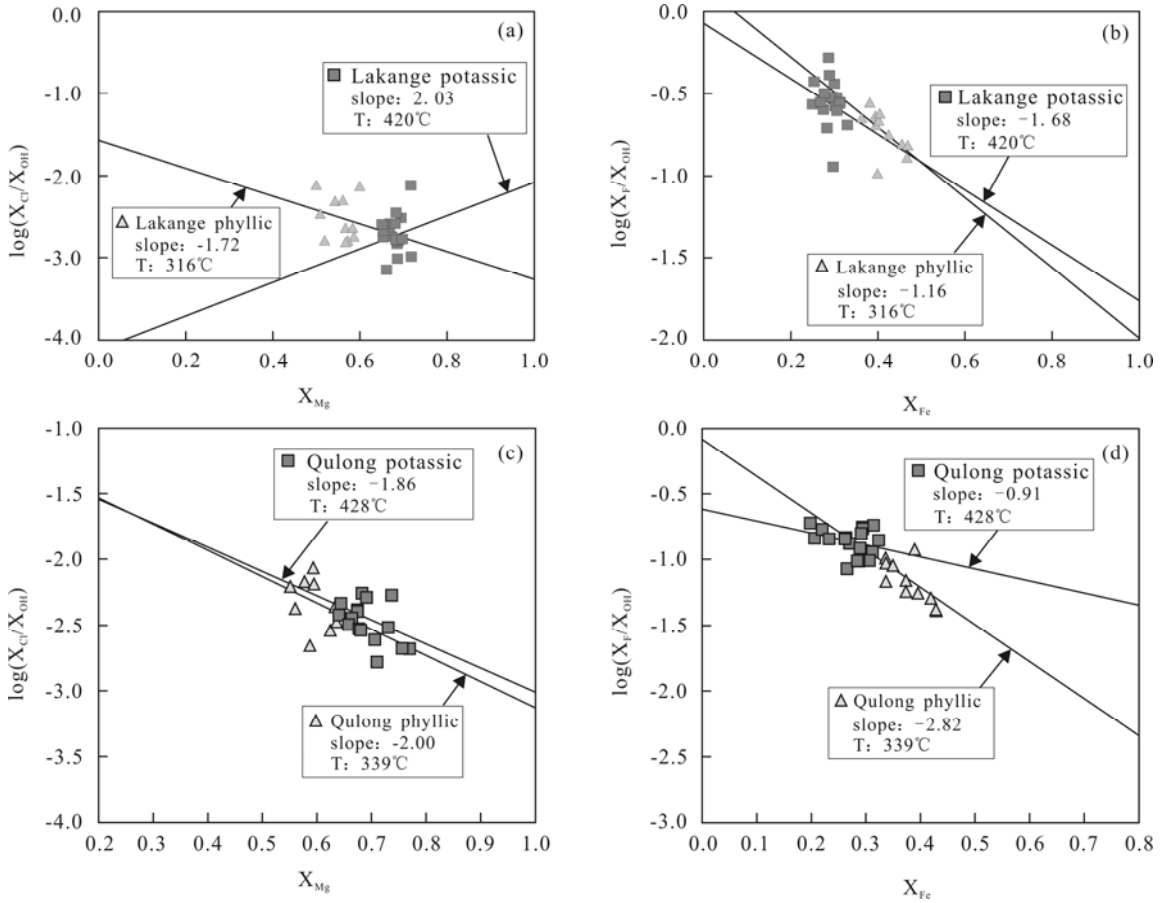


Fig. 10. X_{Mg}–$\log(X_{Cl}/X_{OH})$ and X_{Fe}–$\log(X_F/X_{OH})$ plots for biotites from the Lakange and Qulong deposits.

biotites from porphyry Cu deposits, Sn–W–Be deposits and porphyry Cu deposits, and inferred that porphyry Cu deposits are associated with Cl-rich magmatic system, and porphyry Mo deposits associated with F–rich magmatic system.

The amounts of IV(F) in biotites from the Lakange porphyry Cu–Mo deposit varies between 1.46 and 2.09 (mean=1.77), similar to biotites from other porphyry deposits. The amounts of IV(Cl) in biotites from the Lakange porphyry Cu–Mo deposit varies between −4.29 and −3.10 (mean=−3.62) and is higher than biotites from other porphyry deposits and the Henderson porphyry Mo deposit. The amounts of IV(F/Cl) in biotites from the Lakange porphyry Cu–Mo deposit varies between 4.89 and 5.93 (mean=5.39), partly overprinting other porphyry deposits and the Henderson porphyry Mo deposit (Fig. 11). The biotites from the Lakange deposit fall within the field of the Sn–W–Be and porphyry Mo deposits on the IV (F/Cl)–IV(F) plot (Fig. 12). Therefore, the magmatic system associated with the Lakange porphyry Cu–Mo deposit are richer in F than other porphyry Cu deposits, which is consistent with a large number of fluorite in the Lakange deposit, and richer in Cl than Henderson porphyry Mo deposit. The amounts of IV(F) in biotites from the Qulong porphyry Cu deposit varies between 1.85 to 2.46 (mean= 2.10), similar to biotites from other porphyry deposits. The amounts of IV(Cl) in biotites from the Qulong porphyry Cu deposit varies between −3.89 and −4.18 (mean=−3.89), similar to biotites from other porphyry deposits and the Henderson porphyry Mo deposit. The amounts of IV(F/Cl) in biotites from the Qulong porphyry Cu deposit varies between 5.44 to 6.45 (mean=5.99), similar to biotites from other porphyry deposits (Fig. 11). As in Miduk, Sarcheshmeh, Dalli, Darreh-Zar and Kahang, biotites from the Qulong deposit fall within the field of porphyry Cu deposits on the IV(F/Cl)–IV(F) plot (Fig. 12). Therefore, the Qulong porphyry Cu deposit and other porphyry Cu deposits have similar F and Cl contents.

Mg-rich biotites are characteristic of igneous rocks associated with porphyry copper deposits (Moore and Czamanske, 1973; Taylor, 1983; Selby and Nesbitt, 2000). Biotites related to the porphyry Cu deposits don't generally show obvious Cl-rich (Boomeri et al., 2009; Boomeri et al., 2010; Ayati et al., 2008; Parsapoor et al., 2015; Afshooni et al., 2013； Munoz, 1984), this is because of Mg-rich biotites ("Mg-Cl avoidance") and that the ionic crystal radius of Cl^- (1.81Å) is significantly larger than either F^- (1.31 Å) or OH^- (1.38 Å) so that Cl=OH exchange less than F=OH exchange (Munoz, 1984). Therefore, even if the Cl content in Mg-biotite or phlogopite is very few, it also needs Cl-rich melt or hydrothermal fluid.

Various factors are thought to influence whether a mineralized porphyry system is Mo- or Cu-dominated. Such factors include the composition of the source; the amount of water in the magma; the volatile composition, particularly F/Cl and F/H_2O, of the source and magma, which are partially controlled by the tectonic setting, the depth of emplacement, oxygen fugacity, timing of vapor exsolution, and metal ratio in the source and magma, among others (Beane et al., 1981; Titley et al., 1981; White et al., 1981; Candela et al., 1984;Candela, 1989;

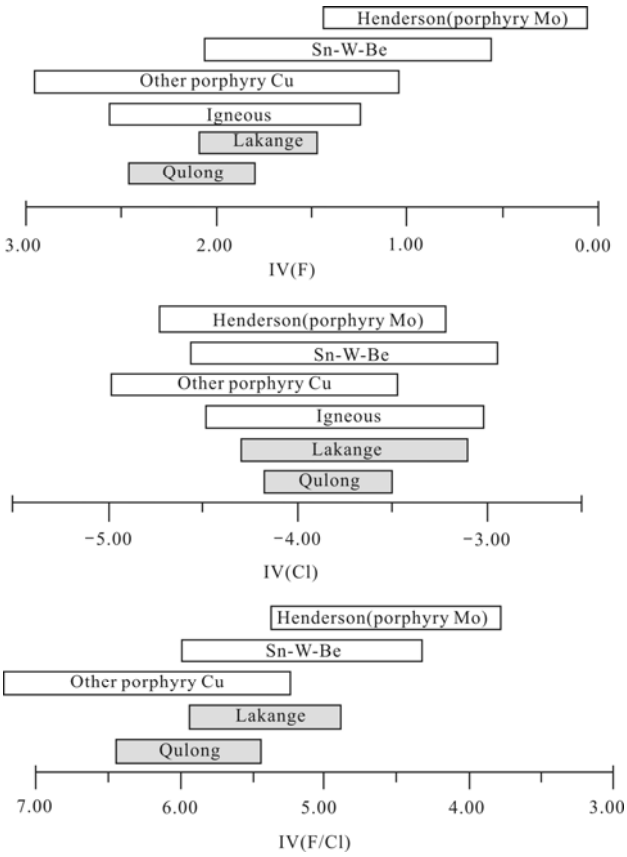


Fig. 11. Comparison of IV(F), IV(Cl), and IV(F/Cl) in Sn–W–Be, Mo, and Cu porphyries (after Parsapoor et al., 2015). The compared data are from Munoz (1984).

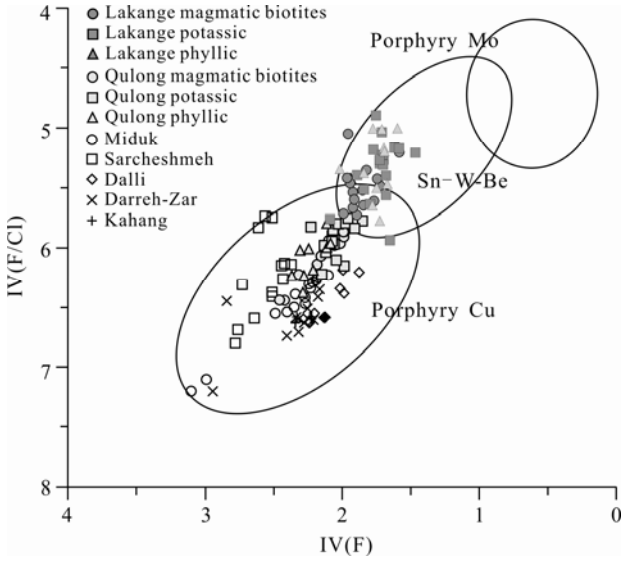


Fig. 12. Compositions of biotites from the Lakange and Qulong deposits on IV(F/Cl) vs. IV(F) diagram (modified from Munoz, 1984； Boomeri et al., 2009).

Miduk, Sarcheshmeh, Dalli, Darreh-Zar and Kahang porphyry copper deposits are taken from Boomeri et al. (2009, 2010), Ayati et al. (2008), Parsapoor et al. (2015) and Afshooni et al. (2013), respectively.

Hannah et al, 1990).

The high F content, F/Cl ratio and F/H_2O ratio of porphyry-Mo magmas may be inherited from the source either by previous melting or by significant dehydration of the source during metamorphism (Loferski et al., 1995). Alternatively, a high F/Cl ratio may be a result of earlier vapor saturation of the magma and resultant loss of Cl, which is strongly partitioned into vapor relative to melt (Loferski et al., 1995). Early vapor saturation would also result in loss of Cu and Mo from the magma because both are partitioned into the vapor phase (Candela and Holland, 1984). Biotites from porphyry-Cu deposits record the relatively high-Cl/F environment of formation. In general, porphyry Cu-related deposits are formed by Cl and alkali rich magmatic hydrothermal fluids that are derived from crystallizing intermediate magmas emplaced into the upper crust associated with plate tectonic convergence (Burnham and Ohmoto, 1980; Sillitoe and Khan, 1977). The high Cl contents indicate that the magmas were not previously vapor saturated. Vapor saturation occurs at a relatively early stage in the crystallization history, and Cu is removed from the melt by complexing with Cl (Candela and Holland, 1984; Candela, 1989).

7.2 Halogen fugacity ratios

Volatile elements (in particular fluorine and chlorine) play an important role in magmatic-hydrothermal ore-forming systems. For example, the halogens affect a variety of processes such as the timing of vapor saturation, and, by complexing with metals, they exert strong controls on the compositional variations and style of mineralization in hydrothermal ore deposits. Consequently, much attention has been focussed on methods of determining the relative fugacities of halogens in igneous and hydrothermal ore-forming systems in order to better understand the role of volatiles in these systems (Munoz and Ludington, 1974; Gunow et al., 1980; Munoz, 1984, 1992; Loferski et al., 1995; 1992; van Middelaar and Keith, 1990; Selby et al., 2000). The fugacity ratios were estimated by using the equations proposed by Munoz (1992), which are based on the revised coefficients for F–Cl–OH partitioning between biotite and either a silicate melt or aqueous fluid phase, equilibrated with biotite composition (Zhu and Sverjensky, 1991, 1992). These equations are:

$$\log[(f\mathrm{H_2O}/f\mathrm{HF})]^{\mathrm{fluid}}=1000/T[2.37+1.1(X_{\mathrm{phl}})^{\mathrm{biotite}}]+0.43-\log(X_{\mathrm{F}}/X_{\mathrm{OH}})^{\mathrm{biotite}}$$

$$\log[(f\mathrm{H_2O}/f\mathrm{HCl})]^{\mathrm{fluid}}=1000/T[1.15+0.55(X_{\mathrm{phl}})^{\mathrm{biotite}}]+0.68-\log(X_{\mathrm{Cl}}/X_{\mathrm{OH}})^{\mathrm{biotite}}$$

$$\log[(f\mathrm{HF}/f\mathrm{HCl})]^{\mathrm{fluid}}=-1000/T[1.22+1.65(X_{\mathrm{phl}})^{\mathrm{biotite}}]+0.25+\log(X_{\mathrm{F}}/X_{\mathrm{Cl}})^{\mathrm{biotite}}$$

where T is the temperature in Kelvin of the halogen exchange, X_{Mg} is the sum of Mg in the octahedral site, and X_F, X_{Cl}, and X_{OH} are the mole fractions of F, Cl, and OH in the hydroxyl site of biotite.

Magmatic biotites and hydrothermal biotites in the potassic and phyllic alteration zones from the Lakange porphyry Cu–Mo deposit have log(*f*HF/*f*HCl) values of −0.58 to 0.19 (mean=−0.28), −1.69 to −0.81 (mean=−1.16), and −2.01 to −0.70 (mean=−1.45), log (*f*H_2O/*f*HCl) values of 4.39 to 5.17 (mean=4.59), 5.12 to 6.00 (mean=5.65), and 5.19 to 6.11 (mean=5.68), and log (*f*H_2O/*f*HF) values of 3.95 to 4.41 (mean=4.25), 5.42 to 6.06 (mean=5.69), and 5.55 to 6.47 (mean=6.08), respectively. The log(*f*HF/*f*HCl) decreases, whereas the log(*f*H_2O/*f*HCl) and log(*f*H_2O/*f*HF) increases gradually from magmatic biotites to hydrothermal biotites in the potassic alteration zones to hydrothermal biotites in the phyllic alteration zones. Magmatic biotites and hydrothermal biotites in the potassic and phyllic alteration zones from the Qulong porphyry Cu deposit have log(*f*HF/*f*HCl) values of −1.31 to −0.28 (mean=−0.64), −1.93 to −1.06 (mean=−1.52), and −2.55 to −1.73 (mean=−2.17), log(*f*H_2O/*f*HCl) values of 4.18 to 4.64 (mean=4.45), 4.99 to 5.69 (mean=5.33), and 5.15 to 5.82 (mean=5.43), and log(*f*H_2O/*f*HF) values of 4.07 to 4.91 (mean=4.41), 5.36 to 6.07 (mean=5.77), and 6.26 to 6.87 (mean=6.52), respectively. The log(*f*HF/*f*HCl) decreases, whereas the log(*f*H_2O/*f*HCl) and log(*f*H_2O/*f*HF) increases gradually from magmatic biotites to hydrothermal biotites in the potassic alteration zones to hydrothermal biotites in the phyllic alteration zones. Therefore, there is a difference between magmatic melt and hydrothermal fluids in the Lakange porphyry Cu–Mo deposit and the Qulong porphyry Cu deposit. The distinct fugacity ratios determined for the hydrothermal fluids relative to those for the potassic and phyllic alteration also suggest that the biotite halogen chemistry does not representative of a single fluid chemistry; the scatter in the few fugacity ratios for potassic and phyllic alteration is suggestive of minor overprinting of the biotite halogen chemistry by late-stage hydrothermal fluids (Fig. 13).

Selby et al. (2000) recalculated the fugacity ratios determined from biotites associated with potassic alteration for the Bingham (analytical data, Parry et al., 1978; Lanier et al., 1978; Bowman et al., 1987), Santa Rita (analytical data, Parry et al., 1979), Los Pelambres and Bakircay (analytical data, Taylor, 1983), and Babine Lake (analytical data, Sheets and Nesbitt, submitted) deposits, and associated with porphyry copper mineralization for the Hanover (analytical data, Jacobs and Parry, 1979) and Deboullie plutons (analytical data, Loferski and Ayuso, 1995) using the equations of Munoz (1992), and compared with the fugacity ratios of Casino porphyry Cu-Au-Mo deposits (Fig. 13). The recalculated fugacity ratios for biotites in the Lakange porphyry Cu–Mo deposit, Qulong porphyry Cu deposit, Miduk, Sarcheshmeh, Dalli, Darreh-Zar, and Kahang porphyry Cu deposits also plot on log(*f*HF/*f*HF)–log(*f*H_2O/*f*HCl) diagram of Selby et al. (2000) (Fig. 13). The above implies that the fluids associated with porphyry-Mo deposits are relatively higher in F/Cl than those associated with porphyry-Cu deposits; log(*f*H_2O/*f*HF) and log(*f*H_2O/*f*HCl) values of hydrothermal biotites from the potassic and phyllic zone are higher than those of magmatic biotites from the Lakange and Qulong deposits, and those of hydrothermal biotites from the phyllic zone are higher than those of the potassic zone from the Lakange, Qulong, Dalli, Sarcheshmeh, Kahang and Casino porphyry deposits.

In the process of magmatic-hydrothermal evolution, the water content increases continuously, and this yields

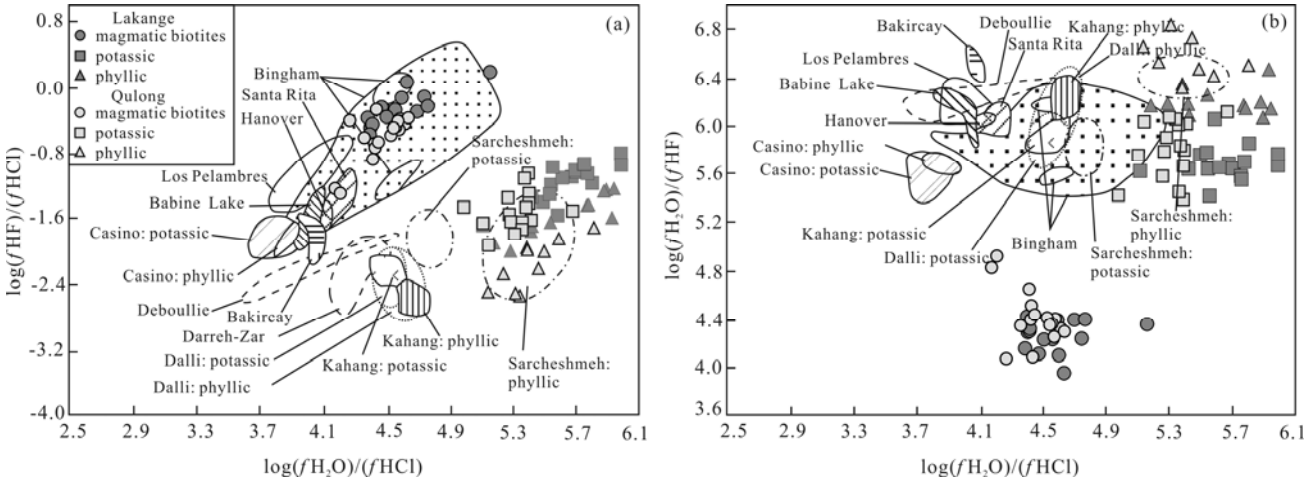


Fig. 13. Comparison of the porphyry systems in terms of (a) log(*f*HF)/(*f*HCl)–log(*f*H_2O)/(*f*HCl) and (b) log(*f*HF)/(*f*HCl)–log(*f*H_2O)/(*f*HF) ratios (modified from Selby et al., 2000; Boomeri et al., 2009; Boomeri et al., 2010; Ayati et al., 2008; Parsapoor et al., 2015; Afshooni et al., 2013).

higher log(*f*H_2O/*f*HCl) and log(*f*H_2O/*f*HF) in hydrothermal biotites. Biotites with high values of log(*f*H_2O/*f*HF) and log(*f*H_2O/*f*HCl) are probably affected by later (cryptic?) meteoric water reaction on exchangeable sites (Selby and Nesbitt, 2000). Therefore, the hydrothermal biotites in the phyllic zone with higher log(*f*H_2O/*f*HCl) and log(*f*H_2O/*f*HF) than potassic zone may be the products of mixing of hydrothermal fluid in the phyllic with meteoric water. As the hydrothermal fluids rise along cracks in porphyry systems, temperature and pressure decrease rapidly. This result in acid-base dissociation and pH decrease, and phyllic acidity increases. Under strong acidic conditions, H^+ reacts with biotite and feldspar to form sericite, clays and sulfides. For decreasing temperature, pressure and oxygen fugacity, and neutralization reaction, sulfides precipitate. HCl and HF dissociation is constant, causing the HCl and HF content in the fluid to decrease. In addition, hydrothermal fluid mix with meteoric water, and consequently the log(*f*H_2O/*f*HF) and log(*f*H_2O/*f*HCl) of hydrothermal biotites from the phyllic zone are higher than those of the potassic zone.

8 Copper Content in Biotite

Since the beginning of the 20th century, copper in biotites from intrusions is an important research field of porphyry copper deposits, and copper in biotites also support the magma genesis model of porphyry deposit (Parry et al., 1963; Al-Hashimi et al., 1970; Grabeal, 1973; Hendry et al., 1981; 1985; Cook, 1988; Ilton et al.,1988; 1993; Liu et al., 1995). Early work was based on optical microscope and minerals analysis, which has large uncertainties because of partial alteration of biotite and sulfide and other mineral inclusions in biotite. Modern work is based on in situ microanalytical techniques, e.g., ion microprobe, electron microprobe, laser plasma mass spectrometer and transmission electron microscopy.

Burns and Fyfe (1964) showed that the Al_2O_3/(K_2O+Na_2O+CaO) of magma is proportional to the number of octahedral sites available in the melt, and copper ions occur in tetrahedral and octahedral coordination in silicate melts but occupy octahedral sites in minerals that crystallize from the melt. Feiss (1978) predicted that copper occur in octahedral blocks in biotite and other mafic minerals by a comparison of the $A1_2O_3$/(K_2O+Na_2O+CaO) of mineralized and barren intrusives from the southwestern U.S. and Caribbean porphyry belts.

Parry et al. (1963) studied biotites from several Basin and Range monzonitic stocks for copper by spectrographic analysis and found that barren intrusions have mean copper content of 10 ppm or less, whereas mineralized intrusions contain more than 50 ppm of copper, and exceptional copper producers above 100 ppm copper. The copper content of biotite is an indicator of Cu mining districts in the Basin and Range province. Grabeal (1973) used atomic absorption spectrophotometer to study Cu concentrations in biotites from two Laramide intrusions in Arizona which vary from 15 to 3658 ppm and noted that Cu content in biotite progressively increase during the early stages of magmatic crystallization and decrease during the later stages, which correlates with Cu fractionation from the melt into hydrothermal phases, indicating that much Cu into hydrothermal phase in the genetically is associated with porphyry deposits. Hendry et al. (1981, 1985) used ion-probe to analyze copper contents in biotites from barren and mineralized intrusions in North American and Solomon Islands porphyry copper deposits and concluded that Cu content in biotites from barren intrusions is higher than those from mineralizing and weak mineralizing intrusions. Thus, they proposed that copper in biotites and other mafic minerals is extracted into hydrothermal fluids to form porphyry copper deposits by precipitation in the later magmatic evolution, whereas barren intrusions do not undergo concentration process.

Al-Hashimi et al. (1970) pointed out that copper content of 61 biotites from rocks of the Late Cretaceous, obtained by instrumental neutron activation analysis, ranges from 6 to 4395 ppm (mean 700 ppm). Very small sulfide inclusions (chalcopyrite, bornite and cuprite) are found in

biotites of several samples by a detailed study of polished thin sections under high magnification and oil immersion, and high copper values is accounted for by the presence of minute inclusions of sulfide minerals in the biotite, rather than to extensive isomorphic substitution of copper in the crystal structure. Ilton and Veblen (1988, 1993) used high-resolution transmission electron microscopy to study the geochemistry of Cu in biotites and noted that anomalous Cu in biotite is present primarily as submicrometre inclusions of pure native Cu in the interlayer regions of the biotite (by X-ray analytical transmission electron microscopy). The Cu inclusions range from 2 to 100 nm in width and are up to ~1000 nm in diameter and were generally flattened parallel to the layers of the enclosing sheet silicate. Deformed hydrobiotie interlayers—expanded interlayer (not identify its composition) contain Cu inclusions.

Cook (1988) used electron microprobe to study the geochemistry of Cu in biotite from supergene zone in the Lakeshore porphyry copper deposit, Arizona, and noted that altered biotite contain high copper content (0.16–8.86 wt%) in supergene zone, associated with hypergenesis. Ilton and Earley (1992) verified weathering effect on copper enrichment in biotite by experiment, and proposed that copper is absorbed into the interlayer region of the biotites where it exchanges for potassium and octahedrally coordinated ferrous iron reduces absorbed copper ions to metallic copper. Ilton and Veblen (1993) used transmission electron microscopy to study copper content in biotites from weathered oxidized and unoxidized rock in the Cyprus Casa Grande porphyry copper deposit, Arizona, and noted that copper-rich biotites and both copper-enriched expanded interlayers and native copper inclusions in biotite are restricted to oxidized rock. Therefore, they concluded that the native copper inclusions and copper-rich expanded interlayers in biotite from Cyprus Casa Grande were formed during weathering and not during hydrothermal event.

Fu (1981) concluded that magmatic biotites generally contain 70–800 ppm copper, mostly less than 30 ppm, whereas hydrothermal biotites contain 450–1100 ppm copper by statistics of different types of biotite from porphyry copper deposits in China. Wang et al. (2012) and Tang et al. (2016), by using laser plasma mass spectrometer and electron microprobe to study copper content in biotites from Jiama porphyry metallogenic system and discovered that the copper content in the hydrothermal biotites is higher than in primary biotites from hornfels and magmatic biotites. Furthermore, they pointed out that the copper content in hydrothermal biotites has an important instruction function for porphyry mineralization.

The microinclusions of Cu minerals may be responsible for some biotites having several thousand ppm Cu. Therefore, it is necessary to understand the effect of microinclusions of Cu minerals to explain copper content in biotite.

9 Evaluation of the Ore-forming Potential

Qin (2009) concluded that biotite composition is associated with the ore potential of porphyry copper deposits, and biotites related to mineralization have the following characteristics. It is Mg-rich and Fe-poor with most Mg/Fe >0.5; high Ti (mostly TiO_2 >3%) and low Al (mostly Al_2O_3<15%); high K and low Na (mostly CaO<0.5%, and K/Na>10); and high Ba, Cu, F, and Cl volatiles. Liu et al. (2010) studied the mineral chemistry of biotite from the Tongshankou porphyry Cu–Mo deposit and pointed out that high oxygen fugacity ($\log fO_2$>NiNiO + 1) in the ore-forming system favors Cu mineralization, and biotites associated with Cu mineralization are characterized by high MgO and low FeO. Dong et al. (2011) showed that the Wushan granodiorite formed at high temperature and oxygen fugacity, and it has large mineralization potential by using biotite mineral chemistry. Xu et al. (2015) showed that the biotites from Shangfanggou and Nanniu stock associated porphyry-skarn Mo polymetallic deposit are Mg-biotite. The crystallization depth of these rocks is 1.4–4.4 km belonging shallow environments, and the crystallization temperature is higher than that for the nonmineralized Laojunshan batholith based on biotite mineral chemistry. Wu et al. (2015) showed that the Huangbeiling porphyritic granite and Zhongyuku monzonitic granite have high temperature and oxygen fugacity, and the hydrothermal fluids related to the two rocks are rich in fluorine based on biotite mineral chemistry, favoring the mineralization of molybdenum and tungsten. Zhang et al. (2016) studied the geochemical characteristics of biotites from felsic intrusive rocks around the Sisson Brook W–Mo–Cu deposit and showed that the biotite granitic dykes have high oxygen fugacity around the nickel–nickel oxide buffer (NNO), whereas other plutonic phases is QFM; if only considering the evolution degree of magma and oxygen fugacity interpreted from the composition of biotite, the magmatic source of the biotite granitic dykes is the plausible source of the hydrothermal fluids responsible for the Sisson Brook deposit mineralization since it has the highest differentiation degree and formed in an oxidized setting.

Li et al. (2007a) studied the mineral chemistry of biotites in the Qitianling granite associated with the Furong tin deposit and showed that the crystallization temperature and oxygen fugacity gradually decrease from hornblende-biotite granite to biotite granite. In addition, the Cl content also gradually decreases and hydrothermal fluids separated during magmatic crystallization become Cl- and Sn-rich with magmatic evolution. As a result, biotite granite is associated with Sn mineralization in the Furong deposit. Li et al. (2007b) studied the mineral chemistry of biotites from the Yanbei pluton and found that the topaz-bearing granite porphyry has high temperature and oxygen fugacity and produce F-rich and Sn-rich fluids during magmatic evolution, which has a closer relation with tin deposit than the topaz-bearing biotite granite. Chen et al. (2015) studied the mineral chemistry of biotites from granite in the Guyong region of Yunnan Province and showed that Xiaolonghe granite form at relatively high temperature, low oxygen fugacity and shallow environment, which has a higher potential for Sn mineralization than the Guyong granite.

Chen et al. (2010) studied the mineral chemistry of biotites in Guidong pluton and showed that the biotites in the Xiazhuang granite are F-rich and crystallize at lower temperature and lower oxygen fugacity than the Luxi granite, which cause that the granite has high uranium content. Therefore, there are many uranium deposits in Xiazhuang granite. Zhang et al. (2011) studied the mineral chemistry of biotites from the uranium-bearing and non uranium-bearing Indosinian granites in south China and showed that compared with the non uranium-bearing granites, the biotites from the uranium-forming granites are strongly altered, contain more accessory mineral inclusions, lower SiO_2, MgO, Fe_2O_3 and TiO_2, and higher F, Al_2O_3 and FeO. Biotites from the uranium-bearing granites are siderophyllite with high $^{VI}Al^{3+}$ and Fe^{2+}, indicating that the uranium-bearing granites are peraluminous and derived from the crust, and have low oxygen fugacity and temperature. These characteristics may be regarded as important indicators for uranium-forming potential of the Indosinian granites in China. Chen et al. (2013) studied the mineral chemistry of biotites from the Guanshigou pegmatite-type uranium deposit in south Shanxi province and showed that biotites from uranium-bearing biotite pegmatites have higher Mg and Mn contents, lower Al, ACNK and oxygen fugacity than other non uranium-bearing pegmatites. Tang et al. (2015) studied the mineral chemistry of biotites from Ziyunshan ore-bearing granite, central Jiangxi, and showed that the Ziyunshan granite formed from F-rich, high temperature and oxygen fugacity favorable for the formation of U and W deposits.

10 Problem

Presently, the composition of biotite from electron microprobe or ion microprobe analysis cannot reproduce Fe^{3+}, Fe^{2+} and OH^-; thus, they have to be calculated (e.g., Dymek, 1983; Zheng et al., 1983; Lin et al., 1994). Although the separation and analysis of single biotites can be used to obtain the FeO and Fe_2O_3 contents, it cannot avoid the inclusions and alteration zones in biotites. The formula of biotite is based on either 22 oxygen atoms or 22+z positive charges. Therefore, the ions in biotite obtained by the different methods also affect the estimated biotite mineral chemistry. Micro-inclusions exist in biotite (copper, nickel and other inclusions) (Al-Hashimi et al., 1970; Ilton et al., 1988; 1993; Warren et al., 2015). Presently, it is difficult to avoid them during routine microanalysis. The presence of copper in the biotite remains controversial mainly because of detection problems. The estimated detection limit for Cu is 200 ppm in electron microprobe analysis and 0.1 wt% in X-ray transmission electron microscopy (Ilton et al., 1988, 1993). Therefore, less than 200 ppm Cu in biotite requires further study.

11 Conclusions

Biotite is an important ferromagnesian silicate mineral that forms during the crystallization of igneous rocks or during hydrothermal alteration. The mineral chemistry of biotite reflects the nature of the magma, hydrothermal alteration and mineralization. Biotite can be used for:

(1) classification;

(2) an indicator for petrogenesis and tectonic setting;

(3) investigating the physicochemical features of ore fluids;

(4) distinguishing between barren and mineralized rocks;

(5) mineral exploration.

Acknowledgments

This work was supported by the National Key R&D Program of China (grant number 2018YFC0604101); the Public Science and Technology Research Funds Projects, Ministry of Land Resources of the People's Republic of China (project nos. 201511017 and 201511022-05); the Basic Research Fund of the Chinese Academy of Geological Sciences (grant no. YYWF201608); the National Natural Science Foundation of China (grant no. 41402178); and the Geological Survey project (grant no. DD20160026). The authors would like to thank anonymous reviewers for their constructive comments and input.

Manuscript received Apr. 13, 2017
accepted Oct. 28, 2018
associate EIC FEI Hongcai
edited by FEI Hongcai

References

Abdel-Rahman, A.M., 1994. Nature of biotites from alkaline, calc-alkaline, and peraluminous magmas. Journal of Petrology, 35(2): 525–541.

Afshooni, S.Z., Mirnejad, H., Esmaeily, D., and Haroni, H.A., 2013. Mineral chemistry of hydrothermal biotite from the Kahang porphyry copper deposit (NE Isfahan), Central Province of Iran. Ore Geology Reviews, 54: 214–232.

Ague, J.J., and Brimhall, G.H., 1988. Regional variations in bulk chemistry, mineralogy, and the compositions of mafic and accessory minerals in the batholiths of California. Geological Society of America Bulletin, 100(100): 891–911.

Al-Hashimi, A.R.K., and Brownlow, A.H., 1970. Copper content of biotites from the Boulder Batholith, Montana. Econonic Geology, 65(8): 985–992.

Abrecht, J., and Hewitt, D.A., 2004. Experimental-evidence on the substitution of ti in biotite. Science of the Total Environment, 327(1–3): 17–30.

Ayati, F., Yavuz, F., Noghreyan, M., Haroni, H.A., and Yavuz, R., 2008. Chemical characteristics and composition of hydrothermal biotite from the Dalli porphyry copper prospect, Arak, central province of Iran. Mineralogy and Petrology, 94 (1–2): 107–122.

Barrière, M., and Cotton, J., 1979. Biotites and associated minerals as markers of magmatic fractionation and deuteric equilibration in granites. Contributions to Mineralogy and Petrology, 70(2): 183–192.

Batchelor, R.A., 2003. Geochemistry of biotite in metabentonites as an age discriminant, indicator of regional magma sources and potential correlating tool. Mineralogical Magazine, 67(4): 807–817.

Beane, R.E., 1974. Biotite stability in the porphyry copper environment. Econonic Geology, 69(2): 241–256.

Boomeri, M., Nakashima, K., and Lentz, D.R., 2010. The Sarcheshmeh porphyry copper deposit, Kerman, Iran: A mineralogical analysis of the igneous rocks and alteration zones including halogen element systematics related to Cu mineralization processes. Ore Geology Reviews, 38(4): 367–

381.
Boomeri, M., Nakashima, K., and Lentz, D.R., 2009. The Miduk porphyry Cu deposit, Kerman, Iran: A geochemical analysis of the potassic zone including halogen element systematics related to Cu mineralization processes. Journal of Geochemical Exploration, 103(1): 17–29.
Burkhard, D.J.M., 1993. Biotite crystallization temperatures and redox states in granitic rocks as indicator for tectonic setting. Geologie en Mijnbouw, 71(4): 337–349.
Burns, R.G., and Fyfe, W.S., 1964. Site of preference energy and selective uptake of transition-metal ions from a magma. Science, 144(3621): 1001–1003.
Chivas, A.R., 1981. Geochemical evidence for magmatic fluids in porphyry copper mineralization. Part I. mafic silicates from the Koloula igneous complex. Contributions to Mineralogy and Petrology, 78(4): 389–403.
Cook, S.S., 1988. Supergene copper mineralization at the Lakeshore mine, Pinal County, Arizona. Economic Geology, 83(2): 297–309.
Coulson, I., Dipple, G., and Raudsepp, M., 2001. Evolution of HF and HCl activity in magmatic volatiles of the gold-mineralized Emerald Lake pluton, Yukon Territory, Canada. Mineralium Deposita, 36(6): 594–606.
Czamanske, G.K., and Wones, D.R., 1973. Oxidation during magmatic differentiation, Finnmarka complex, Oslo Area, Norway: Part 2, the mafic silicates1. Journal of Petrology, 14: 349–380.
Czamanske, G.K., Ishihara, S., and Atkin, S.A., 1981. Chemistry of rock‐forming minerals of the Cretaceous‐Paleocene batholith in southwestern Japan and implications for magma genesis. Journal of Geophysical Research: Solid Earth, 86(11): 10431–10469.
Chen, H.J., Zhang, S.T., Cao, H.W., Wang, X.F., Nie, X.L., Zhang, W., and Tang, L., 2015. Compositional characteristics, petrogenesis and metallogenic significance of biotite from granite in the Guyong region of Western Yunnan Province, China. Acta Mineralogic Sinica, (2): 267–275 (in Chinese with English abstract).
Dahlquist, J.A., Alasino, P.H., Eby, G.N., Galindo, C., and Casquet, C., 2010. Fault controlled Carboniferous A-type magmatism in the proto-Andean foreland (Sierras Pampeanas, Argentina): geochemical constraints and petrogenesis. Lithos, 115(1): 65–81.
De Albuquerque, C.A., 1973. Geochemistry of biotites from granitic rocks, northern Portugal. Geochimica et Cosmochimica Acta, 37(7): 1779–1802.
Dodge, F., Smith, V.C., and Mays, R.E., 1969. Biotites from granitic rocks of the central Sierra Nevada batholith, California. Journal of Petrology, 10(2): 250–271.
Dong, Q., Du, Y.S., Cao, Y., Pang, Z.S., Song, L.X., and Zheng, Z., 2011. Compositional characteristics of biotites in Wushan granodiorite, Jiangxi province: Implications for petrogenesis and mineralization. J Mineral Petrol, 31(2): 1–6 (in Chinese with English abstract).
Douce, A.E.P., 1993. Titanium substitution in biotite: an empirical model with applications to thermometry, O_2 and H_2O barometries, and consequences for biotite stability. Chemical Geology, 108(1–4): 133–162.
El Sheshtawi, Y.A., Salem, A., and Aly, M.M., 1993. The geochemistry of ferrous biotite and petrogenesis of Wadi-El-Sheikh granitoid rocks Southwestern Sinai, Egypt. Journal of African Earth Sciences (and the Middle East), 16(4): 489–498.
Ford, J.H., 1978. A chemical study of alteration at the Panguna porphyry copper deposit, Bougainville, Papua New Guinea. Economic Geology, 73:703–720
Finch, A.A., Parsons, I., and Mingard, S.C., 1995. Biotite as indicators of fluorine fugacities in late-stage magmatic fluids: the Gardar province of south Greenland. Journal of Petrology, 36(6): 1701–1728.
Fu, J.B., 1981. Chemical composition of biotite in porphyry copper deposits. Geology and Prospecting, (9): 16–19 (in Chinese).
Foster, M.D., 1960. Interpretation of the composition of trioctahedral micas. US Geol. Surv. Prof. Pap. 354-B, 1–146.
Feiss, P.G., 1978. Magmatic sources of copper in porphyry copper deposits. Economic Geology, 73(3): 397–404.
Gomes, M.E.P., and Neiva, A.M.R., 2005. Geochemistry of granitoids and their minerals from Rebordelo–Agrochão area, northern Portugal. Lithos, 81(1–4): 235–254.
Gunow, A.J., Ludington, S., and Munoz, J.L., 1980. Fluorine in micas from the Henderson molybdenite deposit, Colorado. Economic Geology, 75(8): 1127–1137.
Guo, Y.Y., He, W.Y., Li, Z.C., Ji, X.Z., Han, Y., Fang, W.K., and Yin, C., 2015. Petrogenesis of Ge'erkuohe porphyry granitoid, western Qinling: Constraints from mineral chemical characteristics of biotites. Acta Petrologica Sinica, 31(11): 3380–3390 (in Chinese with English abstract).
Gao, S.B., Zheng, Y.Y., 2006. Geochemical controlling of mineralization in Qulong super-large porphyry copper deposit, Tibet. Geological Science and Technology Information, 25(2): 41–46 (in Chinese with English abstract).
Hong, D.W., 1982. Biotites and mineralogical facies from granitic rocks of South China and their relation to the series of mineralization. Acta Geologica Sinica, (2): 149–164 (in Chinese with English abstract).
Hu, J., Qiu, J.S., Wang, R.C., Jiang, S.Y., Zing, H.F., Wang, X.L., 2006. Zircon U-Pb geochronology, biotite mineral chemistry and their petrogenetic implications of the Longwo and Baishigang plutons in Guangdong province. Acta Petrologica Sinica, 22(10): 2464–2474
Hendry, D., Chivas, A.R., Long, J., and Reed, S., 1985. Chemical differences between minerals from mineralizing and barren intrusions from some North American porphyry copper deposits. Contributions to Mineralogy and Petrology, 89(4): 317–329.
Hendry, D., Chivas, A.R., Reed, S., and Long, J., 1981. Geochemical evidence for magmatic fluids in porphyry copper mineralization. Part II. Ion-probe analysis of Cu contents of mafic minerals, Koloula igneous complex. Contributions to Mineralogy and Petrology, 78(4): 404–412.
Henry, D.J., 2005. The Ti-saturation surface for low-to-medium pressure metapelitic biotites: Implications for geothermometry and Ti-substitution mechanisms: Implications for geothermometry and Ti-substitution mechanisms. American Mineralogist, 90(2–3): 316–328.
Ilton, E.S., and Veblen, D.R., 1988. Copper inclusions in sheet silicates from porphyry Cu deposits. Nature, 334(6182): 516–518.
Ilton, E.S., and Veblen, D.R., 1993. Origin and mode of copper enrichment in biotite from rocks associated with porphyry copper deposits; a transmission electron microscopy investigation. Economic Geology, 88(4): 885-900.
Jacobs, D.C., and Parry, W.T., 1979. Geochemistry of biotite in the Santa Rita porphyry copper deposit, New Mexico. Econonic Geology, 74(4): 860–887.
Jacobs, D.C., and Parry, W.T., 1976. A comparison of the geochemistry of biotite from some basin and range stocks. Econonic Geology, 71(6): 1029–1035.
Jiang, Y., Jiang, S., Ling, H., Zhou, X., Rui, X., and Yang, W., 2002. Petrology and geochemistry of shoshonitic plutons from the western Kunlun orogenic belt, Xinjiang, northwestern China: implications for granitoid geneses. Lithos, 63(3): 165–187.
Karimpour, M.H., Stern, C.R., and Mouradi, M., 2011. Chemical composition of biotite as a guide to petrogenesis of granitic rocks from Maherabad, Dehnow, Gheshlagh, Khajehmourad and Najmabad, Iran. Iranian Society of Crystallography and Mineralogy, 18: 89–100.
Kesler, S.E., Issigonis, M.J., Brownlow, A.H., Damon, P.E., Moore, W.J., Northcote, K.E., and Preto, V.A., 1975. Geochemistry of biotites from mineralized and barren intrusive systems. Econonic Geology, 70(3): 559–567.
Kanisawa, S., 1983. Chemical characteristics of biotites and hornblendes of Late Mesozoic to Early Tertiary granitic rocks in Japan. Geological Society of America Memoirs, 159:129–134.
Kumar, S., and Pathak, M., 2010. Mineralogy and geochemistry of biotites from Proterozoic granitoids of western Arunachal Himalaya: Evidence of bimodal granitogeny and tectonic

affinity. Journal of the Geological Society of India, 75(5): 715–730.

Leng, Q.F., Tang, J.X., Zheng, W.B., Wang, B.H., Tang, P., and Wang, H., 2016. Geochronology, geochemistry and zircon Hf isotopic compositions of the ore-bearing porphyry in the Lakange porphyry Cu–Mo Deposit, Tibet. Earth Science, 41 (6): 999–1015 (in Chinese with English abstract).

Leng, Q.F., Tang, J.X., Zheng, W.B., Lin, B., Tang, P., Wang, H., and Li, H.F., 2006. Zircon U-Pb and molybdenite Re-Os ages of the Lakange porphyry Cu–Mo deposit, Gangdese Porphyry Copper Belt, Southern Tibet, China. Resource Geology, 66(2): 163–182.

Li, H.L., Bi, X.W., Tu, G.C., Hu, R.Z., Pen, J.T., and Wu, K.X., 2007a. Mineral chemistry of biotite from Yanbei pluton: implication for Sn-metallogeny. J Mineral Petrol, 27(3): 49–54 (in Chinese with English abstract).

Li, H.L., Bi, X.W., Hu, R.Z., Peng, J.T., Shuang, Y., Li, Z.L., Li, X.M., and Yuan, S.D., 2007b. Mineral chemistry of biotite in the Qitianling granite associated with the Furong tin deposit: Tracing tin mineralization signatures. Acta Petrologica Sinica, 23(10): 2605–2614 (in Chinese with English abstract).

Liu, B., Ma, C.Q., Liu, Y.Y., and Xiong, F.H., 2010. Mineral chemistry of biotites from the Tongshankou Cu–Mo deposit: Implications for petrogenesis and mineralization. Acta Petrologica et Mineralogica, 29(2): 151–165 (in Chinese with English abstract).

Lou, Y.E., Du, Y.S., 2006. Characteristics and genesis of biotites from the Mesozoic intrusive rocks in the Fanchang- Tongling area, Anhui province. Acta Mineralogica Sincia, 26(2): 175–180 (in Chinese with English abstract).

Liu, L.J., Wang, J.C., 1984. The formative mechanism of biotitization-biotite—recrystallization in granitoid and its geological significance. Geoteconica et Metallogenia, 8(4): 369–375 (in Chinese with English abstract).

Lalonde, A., 1993. Composition and color of biotite from granites two useful properties in the characterization of plutonic suites from the Hepburn internal zone of Wopmay orogeny, Northwest Territories. Canadian Mineralogist, 31: 203–217.

Lanier, G., Raab, W.J., Folsom, R.B., and Cone, S., 1978. Alteration of equigranular monzonite, Bingham mining district, Utah. Economic Geology, 73(7): 1270–1286.

Lentz, D., 1992. Petrogenesis and geochemical composition of biotites in rare-element granitic pegmatites in the southwestern Grenville Province, Canada. Mineralogy and Petrology, 46(3): 239–256.

Loferski, P.J., and Ayuso, R.A., 1995. Petrography and mineral chemistry of the composite Deboullie pluton, northern Maine, USA: Implications for the genesis of Cu–Mo mineralization. Chemical Geology, 123(1): 89–105.

Liu, S.B., and Wang, L.K., 1995. Advances in the research of copper in biotites from intrusive rocks. Geological Science and Technology Information, 14(3): 67–72 (in Chinese with English abstract).

Moore, W.J., and Czamanske, G.K., 1973. Compositions of biotites from unaltered and altered monzonitic rocks in the Bingham Mining District, Utah. Economic Geology, 68(2): 269–274.

Munoz, J.L., 1984. F-OH and Cl-OH exchange in micas with applications to hydrothermal ore deposits. Reviews in Mineralogy and Geochemistry, 13(1): 469–493.

Munoz, J.L., 1992. Calculation of HF and HCl fugacities from biotite compositions: revised equations. Geological Society of America, Abstracts with Programs, 24, A221.

Munoz, J.L., and Ludington, S.D., 1974. Fluoride-hydroxyl exchange in biotite. American Journal of Science, 274(4): 396-413.

Munoz, J.L., and Swenson, A., 1981. Chloride-hydroxyl exchange in biotite and estimation of relative HCl/HF activities in hydrothermal fluids. Economic Geology, 76(8): 2212–2221.

Mi, J.R., Yuan, S.D., Yuan, Y.B., and Xuan, Y.S., 2014. Mineral chemistry of biotites in Baoshan granodiorite_porphyry，southern Hunan Province: Implications for petrogenesis and mineralization. Mineral Deposits, 33(6): 1357–1365 (in Chinese with English abstract).

Nachit, H., Ibhi, A., Abia, E.H., and Ben Ohoud, M., 2005. Discrimination between primary magmatic biotites, reequilibrated biotites and neoformed biotites. Comptes Rendus Geoscience, 337(16): 1415–1420.

Nachit, H., Razafimahefa, N., Stussi, J.M., and Carron, J.P., 1985. Composition chimique des biotites et typologie magmatique des granitoides. Comtes Rendus Hebdomadaires de I' Académie des sciences, 301(11): 813–818.

Neiva, A.R., 1981. Geochemistry of hybrid granitoid rocks and of their biotites from Central Northern Portugal and their petrogenesis. Lithos, 14(2): 149–163.

Niu, X.L., Yang, J.S., Feng, G.Y., and Liu, F., 2015. Mineral chemistry of biotites from the Fanshan ultramafic-syenitic complex from the Fanshan and its petrogenetic significance. Acta Geologica Sinica, 89(6): 1108–1119 (in Chinese with English abstract).

Parry, W.T., and Nackowski, M.P., 1963. Copper, lead, and zinc in biotites from Basin and Range quartz monzonites. Econonic Geology, 58(7): 1126–1144.

Patino Douce, A.E., 1993. Titanium substitution in biotite: an empirical model with applications to thermometry, O_2 and H_2O barometers, and consequence for biotite stability. Chemical Geology, 108: 132–162.

Parsapoor, A., Khalili, M., Tepley, F., and Maghami, M., 2015. Mineral chemistry and isotopic composition of magmatic, re-equilibrated and hydrothermal biotites from Darreh-Zar porphyry copper deposit, Kerman (Southeast of Iran). Ore Geology Reviews, 66: 200–218.

Qin, K.Z., Zhang, L.C., Ding, K.S., Xu, Y.X., Tang, D.M., Xu, X.W., Ma, T.L., and Li, G.M., 2009. Mineralization type, Petrogenesis of ore-bearing intrusions and mineralogical characteristics of Sanchakou copper deposits in eastern Tianshan. Acta Petrologica Sinica, 25(4): 845–861 (in Chinese with English abstract).

Robert, J.L., 1976. Titanium solubility in synthetic phlogopite solid solutions. Chemical Geology, 17(3): 213–227.

Rieder, M., Cavazzini, G., D'Yakonov, Y.S., Frank-Kamenetskii, V.A., Gottardi, G., Guggenheim, S., Koval, P.V., Müller, G., Neiva, A.M.R., Radoslovich, E.W., Robert, J.L., Sassi, F.P., Takeda, H., Weiss, Z., and Wones, D. R., 1998. Nomenclature of themicas. Canadian Mineralogist, 36: 905–912.

Sallet, R., 2000. Fluorine as a tool in the petrogenesis of quartz-bearing magmatic associations: Applications of an improved F-OH biotite-apatite thermometer grid. Lithos, 50(1–3): 241–253.

Sarjoughian, F., Kananian, A., Ahmadian, J., and Murata, M., 2015. Chemical composition of biotite from the Kuh-e Dom pluton, Central Iran: implication for granitoid magmatism and related Cu–Au mineralization. Arabian Journal of Geosciences, 8(3): 1521–1533.

Selby, D., and Nesbitt, B.E., 2000. Chemical composition of biotite from the Casino porphyry Cu–Au–Mo mineralization, Yukon, Canada: evaluation of magmatic and hydrothermal fluid chemistry. Chemical Geology, 171(1–2): 77-93.

Shabani, A.A., Lalonde, A.E., and Whalen, J.B., 2003. Composition of biotite from granitic rocks of the Canadian Appalachian orogen: a potential tectonomagmatic indicator? The Canadian Mineralogist, 41(6): 1381–1396.

Siahcheshm, K., Calagari, A.A., Abedini, A., and Lentz, D.R., 2012. Halogen signatures of biotites from the Maher-Abad porphyry copper deposit, Iran: characterization of volatiles in syn-to post-magmatic hydrothermal fluids. International Geology Review, 54(12): 1353–1368.

Speer, J.A., 1981. Petrology of cordierite-and almandine-bearing granitoid plutons of the southern Appalachian Piedmont, USA. Canadian. Mineralogy, 19: 35–46.

Speer, J.A., 1984. Micas in igneous rocks. Reviews in Mineralogy and Geochemistry, 13(1): 299–356.

Speer, J.A., 1987. Evolution of magmatic AFM mineral assemblages in granitoid rocks: The hornblende + melt = biotite reaction in the Liberty Hill pluton, South Carolina. American Mineralogist, 72(9–10): 863–878.

Taylor, R.P., 1983. Comparison of biotite geochemistry of Bakircay, Turkey, and Los Pelambres, Chile, porphyry copper

systems. Institution of Mining and Metallurgy Transactions, 92: 16–22
Tischendorf, G., Gottesmann, B., Förster, H.J., Trumbull, R.B., 1997. On Li-bearing micas: estimating Li from electron microprobe analyses and an improved diagram for graphical representation. Mineral Magazine, 61: 809–834.
Tischendorf, G., Förster, H., and Gottesmann, B., 2001. Minor- and trace-element composition of trioctahedral micas: a review. Mineralogical Magazine, 65(2): 249–276.
Tang, P., Tang, J.X., Lin, B., Wang, L.Q., Zheng, W.B., Leng, Q.F., Gao, X., Zhang, Z.B., and Tang, X.Q., 2019. Mineral chemistry of magmatic and hydrothermal biotites from the Bangpu porphyry Mo (Cu) deposit, Tibet, Ore Geology Reviews, https://doi.org/10.1016/j.oregeorev.2019.103122.
Tang, P., Chen, Y.C., Tang, J.X., Zheng, W.B., Leng, Q.F., Lin, B., and Fang, X., 2016. Typomorphic characteristics and geological significance of biotites in Jiama porphyry deposit system, Tibet. Mineral Deposits, 35(4): 846–866 (in Chinese with English abstract).
Tang, P., Tang, J.X., Zheng, W.B., Leng, Q.F., Lin, B., and Tand, X.Q., 2017. Mineral chemistry of hydrothermal biotites from the Lakange porphyry Cu-Mo deposit, Tibet. Earth Science Frontier, 24(5): 265–282 (in Chinese with English abstract).
Tang, A., Li, G.L., Zhou, L.Q., and Su, Y., 2015. Compositional characteristics of bioite in Ziyunshan ore bearing granite, central Jiangxi: Implications for petrogenesis and mineralization. Journal of Mineral Petrology, 35(3): 29–34 (in Chinese with English abstract).
Tao, J.H., Cen, T., Long, W.G., and Li, W.X., 2015. Mineral chemistry of biotites from the Indosinian weakly peraluminous and strongly peraluminous granites in South China a and their constraints petrogenesis. Earth Science Frontiers, 22(2): 64–78 (in Chinese with English abstract).
Uchida, E., Endo, S., and Makino, M., 2007. Relationship between solidification depth of granitic rocks and formation of hydrothermal ore deposits. Resource Geology, 57(1): 47–56.
Van Middelaar, W.T., and Keith, J.D., 1990. Mica chemistry as an indicator of oxygen and halogen fugacities in the CanTung and other W-related granitoids in the North American Cordillera. Geological Society of America Special Papers, 246: 205–220.
Whalen, J.B., and Chappell, B.W., 1988. Opaque mineralogy and mafic mineral chemistry of I-and S-type granites of the Lachlan fold belt, southeast Australia. American Mineralogist, 73(3–4): 281–296.
Wones, D.R., and Eugster, H.P., 1965. Stability of biotite-experiment theory and application. American Mineralogist, 50 (9): 1228.
Wang, W.P., Tang, J.X., and Ying, L.J., 2012. Mineral chemical characteristics of biotites from hornfels in the Jiama(Gyama) polymetallic copper deposit of Tibet and their geological significance. Acta Geoscientica Sinica, 33(4): 444–458 (in Chinese with English abstract).
Wang, X.X., and Lu, X.X., 1998. A study of biotite from the Shahewan Rapakivi granite in Qinling and its Significance. Acta Petrologica et Mineralogica, 17(4): 352–358 (in Chinese with English abstract).
Wang, L.L., Mo, X.X., Li, B., Dong, G.C., and Zhao, Z.D., 2006. Geochronology and geochemistry of the ore-bearing porphyry in Qulong Cu(Mo) ore deposit, Tibet. Acta Petrologica Sinica, 22(4): 1001–1008 (in Chinese with English abstract).
Wu, Z.L., Zhang, S.T., Xu, T., Cao, H.W., Pei, Q.M., Deng, M.Z., Tang, C.H., and Zhang, P., 2015. Compositional characteristics, petrogenesis and metallogenic significance of biotite from granite in the Huangbeiling-Zhongyuku region of Luanchuan ore concentration area. Journal of Mineral Petrology, 35(3): 11–19 (in Chinese with English abstract).
Xu, K.Q., and Tu, G.C., 1986. Relationship between Granitic Rocks and Mineralization. Nanjing: Science and Technology of Jiangsu Press, 1–645 (in Chinese).
Xu, T., Zhang, S.T., Yang, B., Cao, H.W., Zhang, Y.H., Pei, Q.M., Zhang, P., Tang, C.H., and Wu, Z.L., 2015. Characteristics of biotites in two types of Yansahnian granitic pluton in Luanchuan ore concentration area of China and its significance. Journal of Chengdu University of Technology (Science & Technology Edition), 42(3): 257–267 (in Chinese with English abstract).
Xiong, X.L., Shi, M.Q., and Chen, F.R., 2001. Biotite as A tracer of Cu and Au mineralization in hypergene - subvolcanic plutons. Mineral Deposits, 21(2): 107-111 (in Chinese with English abstract).
Yang, M.Z., 1964. The alteration of hydrothermal biotite in disseminated molybdenum deposits, Eastern China. Acta Geologica Sinica, 44(2): 191–212 (in Chinese with English abstract).
Yang, X., and Lentz, D.R., 2005. Chemical composition of rock-forming minerals in gold-related granitoid intrusions, southwestern New Brunswick, Canada: implications for crystallization conditions, volatile exsolution, and fluorine-chlorine activity. Contributions to Mineralogy and Petrology, 150(3): 287–305.
Yavuz, F., 2003a. Evaluating micas in petrologic and metallogenic aspect: Part II—Applications using the computer program Mica+. Computers & Geosciences, 29(10): 1215–1228.
Yavuz, F., 2003b. Evaluating micas in petrologic and metallogenic aspect: I–definitions and structure of the computer program MICA. Computers & Geosciences, 29(10): 1215–1228.
Zhu, C., and Sverjensky, D.A., 1991. Partitioning of F-Cl-OH between minerals and hydrothermal fluids. Geochimica et Cosmochimica Acta, 55(7): 1837–1858.
Zhu, C., and Sverjensky, D.A., 1992. F-Cl-OH partitioning between biotite and apatite. Geochimica et Cosmochimica Acta, 56(9): 3435–3467.
Zhang, P.P., and Zhu, Z.X., 1991. The mineralogical characteristics of biotites in granite and its genetic significance in central and southern Daxinganling mountains. Journal of Changchun University of Earth Science, 21(3): 307 –312 (in Chinese with English abstract).
Zhang, J., Chen, W.F., and Chen, P.R., 2011. Compositional differences of the biotites from the uranium-forming and non uranium-forming Indosinian Granites in South China. Geotectonica et Metallogenia, 35(2): 270–277 (in Chinese with English abstract).
Zhou, Z.X., 1986. The origin of intrusive mass in Fengshandong, Hubei province. Acta Petrotogica Sinica, 2(1): 59–70 (in Chinese with English abstract).
Zhang, W., Lentz, D.R., Thorne, K.G., and McFarlane, C., 2016. Geochemical characteristics of biotite from felsic intrusive rocks around the Sisson Brook W–Mo–Cu deposit, west-central New Brunswick: An indicator of halogen and oxygen fugacity of magmatic systems. Ore Geology Reviews, 77: 82–96.

About the first author



TANG Pan, male, was born in 1989 in Sichuan province, and is a postdoctor at Faculty of Geosciences and Environmental Engineering, Southwest Jiaotong University. He is now interested in the research of exploration and evaluation of porphyry-skarn deposit.

About the corresponding author



TANG Juxing, male; born in 1964 in Zhejiang Province; is a researcher of Institute of Mineral Resources, Chinese Academy of Geological Sciences. He is now interested in study of mineral deposit and exploration in the main metallogenic belt, Tibet. Email: tangjuxing@126.com.